NAVAL POSTGRADUATE SCHOOL
Monterey, California

THESIS

A DIAGNOSTIC STUDY OF THE VELOCITY
STRUCTURE OF A MEANDERING
JET USING A PRIMITIVE EQUATION MODEL
WITH DYNAMIC MODE INITIALIZATION

by

Roland E. de Jesus

September 1990

Thesis Advisor	R. L. Haney
Co-Advisor	T. P. Stanton

Approved for public release; distribution is unlimited.

91-11303

91 9 23 045

REPORT DOCUMENTATION PAGE

1a Report Security Classification Unclassified	1b Restrictive Markings

2a Security Classification Authority	3 Distribution Availability of Report
2b Declassification Downgrading Schedule	Approved for public release; distribution is unlimited.

4 Performing Organization Report Number(s)	5 Monitoring Organization Report Number(s)

6a Name of Performing Organization Naval Postgraduate School	6b Office Symbol (if applicable) 35	7a Name of Monitoring Organization Naval Postgraduate School

6c Address (city, state, and ZIP code) Monterey, CA 93943-5000	7b Address (city, state, and ZIP code) Monterey, CA 93943-5000

8a Name of Funding Sponsoring Organization	8b Office Symbol (if applicable)	9 Procurement Instrument Identification Number

8c Address (city, state, and ZIP code)	10 Source of Funding Numbers			
	Program Element No	Project No	Task No	Work Unit Accession No

11 Title (Include security classification) A DIAGNOSTIC STUDY OF THE VELOCITY STRUCTURE OF A MEANDERING JET USING A PRIMITIVE EQUATION MODEL WITH DYNAMIC MODE INITIALIZATION

12 Personal Author(s) Roland E. de Jesus

13a Type of Report Master's Thesis	13b Time Covered From To	14 Date of Report (year, month, day) September 1990	15 Page Count 77

16 Supplementary Notation The views expressed in this thesis are those of the author and do not reflect the official policy or position of the Department of Defense or the U.S. Government.

17 Cosati Codes			18 Subject Terms (continue on reverse if necessary and identify by block number)
Field	Group	Subgroup	diagnostic model, California Current, CTZ, dynamical modes

19 Abstract (continue on reverse if necessary and identify by block number)

A high resolution, 20-level, primitive equation (PE) model of the California coastal region is initialized using temperature data acquired during the first Naval Postgraduate School California Transition Zone (CTZ) cruise from 6 to 12 July 1988 for the purpose of diagnosing the three-dimensional dynamically balanced flow field for the region. The major feature in the region during the cruise period was a strong meandering jet which flowed equatorward and offshore, oriented in a northeast to southwest direction. The quality of data acquired during cruise CTZR1 is sufficiently high to enable diagnosis of the horizontal (baroclinic) and vertical velocity field using the numerical model. The measured (ADCP) currents showed more details of the flow at deeper depths than the model, which showed a broader baroclinic flow at depth and a level of no motion near 300 m. The maximum surface velocities from model and ADCP cross-sections agreed to within 10 cm sec^{-1} except for leg G, in which ADCP velocity was greater than the model velocity by about 30 cm sec^{-1}. The sign of vertical velocity agrees very well with independent estimates made from bio-optical data; however, the magnitude calculated by the model is 30 to 60 times larger than that estimated from the bio-optical observations.

20 Distribution Availability of Abstract			21 Abstract Security Classification
☒ unclassified unlimited ☐ same as report ☐ DTIC users			Unclassified

22a Name of Responsible Individual R. L. Haney	22b Telephone (include Area code) (408) 646-2517	22c Office Symbol Code MR/Hy

A Diagnostic Study of the Velocity Structure of a Meandering
Jet Using a Primitive Equation Model with Dynamic Mode Initialization

by

Roland E. de Jesus
Lieutenant Commander, United States Navy
B.S., U. S. Naval Academy, 1980

Submitted in partial fulfillment of the
requirements for the degree of

MASTER OF SCIENCE IN METEOROLOGY AND PHYSICAL OCEANOGRAPHY

from the

NAVAL POSTGRADUATE SCHOOL
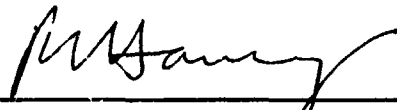September 1990

Author: _____

Roland E. de Jesus

Approved by: _____

R. L. Haney, Thesis Advisor

_____

T. P. Stanton, Co-Advisor

_____

Robert L. Haney, Chairman,
Department of Meteorology

ii

ABSTRACT

A high resolution, 20-level, primitive equation (PE) model of the California coastal region is initialized using temperature data acquired during the first Naval Postgraduate School California Transition Zone (CTZ) cruise from 6 to 12 July 1988 for the purpose of diagnosing the three-dimensional dynamically balanced flow field for the region. The major feature in the region during the cruise period was a strong meandering jet which flowed equatorward and offshore, oriented in a northeast to southwest direction. The quality of data acquired during cruise CTZR1 is sufficiently high to enable diagnosis of the horizontal (baroclinic) and vertical velocity field using the numerical model. The measured (ADCP) currents showed more details of the flow at deeper depths than the model, which showed a broader baroclinic flow at depth and a level of no motion near 300 m. The maximum surface velocities from model and ADCP cross-sections agreed to within 10 cm sec^{-1} except for leg G, in which ADCP velocity was greater than the model velocity by about 30 cm sec^{-1}. The sign of vertical velocity agrees very well with independent estimates made from bio-optical data, however, the magnitude calculated by the model is 30 to 60 times larger th .n that estimated from the bio-optical observations.

iii

TABLE OF CONTENTS

LIST OF TABLES

LIST OF FIGURES

ACKNOWLEDGEMENTS

I. INTRODUCTION

A. THE CALIFORNIA CURRENT SYSTEM

The California Current is the equatorward leg of the anticyclonic gyre covering the majority of the North Pacific between 5° to 10° N and 45° to 50° N (Tchernia, 1980). The core of the mean California Current is located approximately 100 to 200 km offshore in the upper 200 m. Current velocities range from 5 cm sec^{-1} to 14 cm sec^{-1} depending on the season and location (Chelton, 1984). Chelton calculated these velocities using geostrophy, with 500 m as the level of no motion. Over 30 years of hydrographic survey data from California Cooperative Oceanic Fisheries Investigations between San Francisco and Point Conception were used in his study. In addition to the equatorward flowing California Current there exists the poleward flowing, subsurface California Undercurrent; the poleward flowing, surface Davidson Current, found north of Point Conception during fall and winter; and the poleward flowing, surface Southern California Countercurrent, found south of Point Conception in the California Bight. These four currents make up the California Current System (CCS). Hickey (1979) provides a thorough description of the seasonal variation of the currents in the CCS.

The CCS is important to the climate and economy of the west coast states. Upwelling events bring up cold, nutrient-rich subsurface water to the ocean surface, providing nourishment to the phytoplankton in the euphotic zone (Brink, 1983; Huyer, 1983; Parsons et a', 1977). The cool sea-surface temperatures adjacent to the coast engenders mild weather conditions and the ocean provides moisture for the surface boundary layer, promoting cloud formation and fog (Foster, 1989). Additionally, surface salinity fronts bounding the offshore edge of a meandering jet; temperature fronts; and sharp, near-surface density fronts associated with upwelling affect sonar performance in fleet operating areas. The continuing study of the CCS, representing a typical eastern boundary current, is necessary for the promotion of both military and civilian interests.

Interesting features of the CCS are the cold filaments occurring off the west coast of the United States, as far north as Vancouver Island, British Columbia and as far south as Point Conception, California (Ikeda and Emery, 1984). These filaments (also known as tongues, jets, or squirts) consist of cold, salty inshore water which has been carried offshore, beyond the continental shelf (Brink, 1983; CTZ Group, 1988; Ikeda and Emery,

1

1984). Summer infrared satellite images from the West Coasts of California and Oregon have shown these filaments extending westward from the coast (Ikeda and Emery, 1984; CTZ Group, 1988; Ramp and Jessen, 1988; Stanton and Stockel, 1988).

The purpose of the Coastal Transition Zone (CTZ) program is to investigate the cold filaments associated with the CCS. Four major goals of the CTZ program are to understand the processes involved in the interaction of the filaments with open ocean water; determine the effect of the filaments on the biology and meteorology of the coastal zone; create a series of maps of the current, hydrographic, nutrient, and particle fields; and discover, through use of numerical models, what driving forces, dynamics, topography, and stratification is necessary to duplicate the observed characteristics of these filaments (CTZ Group, 1988).

B. OBJECTIVE

The objective of this thesis is to diagnose the velocity fields from acquired temperature data in the region off Point Arena from approximately 37°10′ to 39°21′N and 123°50′ to 126°40′W, which covers roughly one meander of the California Current. Areas of convergence and divergence and their relation with the diagnosed vertical velocity fields will be examined. Knowledge of the velocity fields is important to tracer studies, and the vertical velocity field is of continuing interest to biologists and the local fisheries industry.

II. THE MODEL

The numerical model is a 20-level, primitive equation model of a baroclinic ocean on an f-plane, with hydrostatic, Boussinesq, and rigid lid approximations. The space-staggered B-scheme (Messinger and Arakawa, 1982) is used for horizontal finite differencing, and a sigma coordinate system defines the vertical dimension. The boundary conditions at the sea surface consist of no wind stress and no heat flux. The lateral boundaries of the model domain are treated as open boundaries using the method of Ross and Orlanski (1983). The total depth of the ocean is 4000 m, with model levels listed in Table 1. The values of constants used in the model are listed in Table 2. No attempt is made to model the depth averaged part of the currents which are taken to be zero.

Table 1. K-LEVELS AND CORRESPONDING DEPTHS IN ME-
TERS USED IN MODEL

k level	z(k) (meters)	k level	z(k) (meters)
1	5	11	1105
2	25	12	1325
3	65	13	1565
4	125	14	1825
5	205	15	2105
6	305	16	2405
7	425	17	2725
8	565	18	3065
9	725	19	3425
10	905	20	3805

Table 2. CONSTANTS USED IN MODEL

Constant	Value	Name
Ω	$2\pi\ day^{-1}$	earth rotation rate
DTAU	600 s	timestep
dx	4×10^5 cm	meridional grid spacing
dy	4×10^5 cm	zonal grid spacing
D	4×10^5 cm	total ocean depth
LAT	38.25' N	reference latitude
f	9.00×10^{-5} sec^{-1}	Coriolis parameter
g	$980\ cm$ sec^{-2}	acceleration of gravity
A_M	$4 \times 10^{17}\ cm^4$ sec^{-1}	biharmonic momentum diffusion coefficient
A_H	$4 \times 10^{17}\ cm^4$ sec^{-1}	biharmonic heat diffusion coefficient
K_M	$0.5\ cm^2$ sec^{-1}	vertical eddy viscosity
K_H	$0.5\ cm^2$ sec^{-1}	vertical eddy conductivity
α	$2.877 \times 10^{-4}\ C^{-1}$	thermal expansion coefficient

The chart of the 1988 CTZ station grid is shown in Figure 1. The station grid extends approximately 120 nm offshore and 110 nm alongshore, roughly parallel to the California coast and southwest of Point Arena. The alongshore sections are approximately 20 nm apart and have individual stations approximately 13 to 14 nm apart. The model domain covers the area from 37'10' to 39'21'N and 123'50' to 126'40'W. The chart of the model domain with included stations is shown in Figure 2. The model domain excludes stations A1, A2, A3, A4, A5, B8, and B9. The actual topography in the model domain is shown in Figure 3. The effect of variable topography and depth averaged currents, as well as wind forcing and surface heat fluxes is considered a separate study.

4
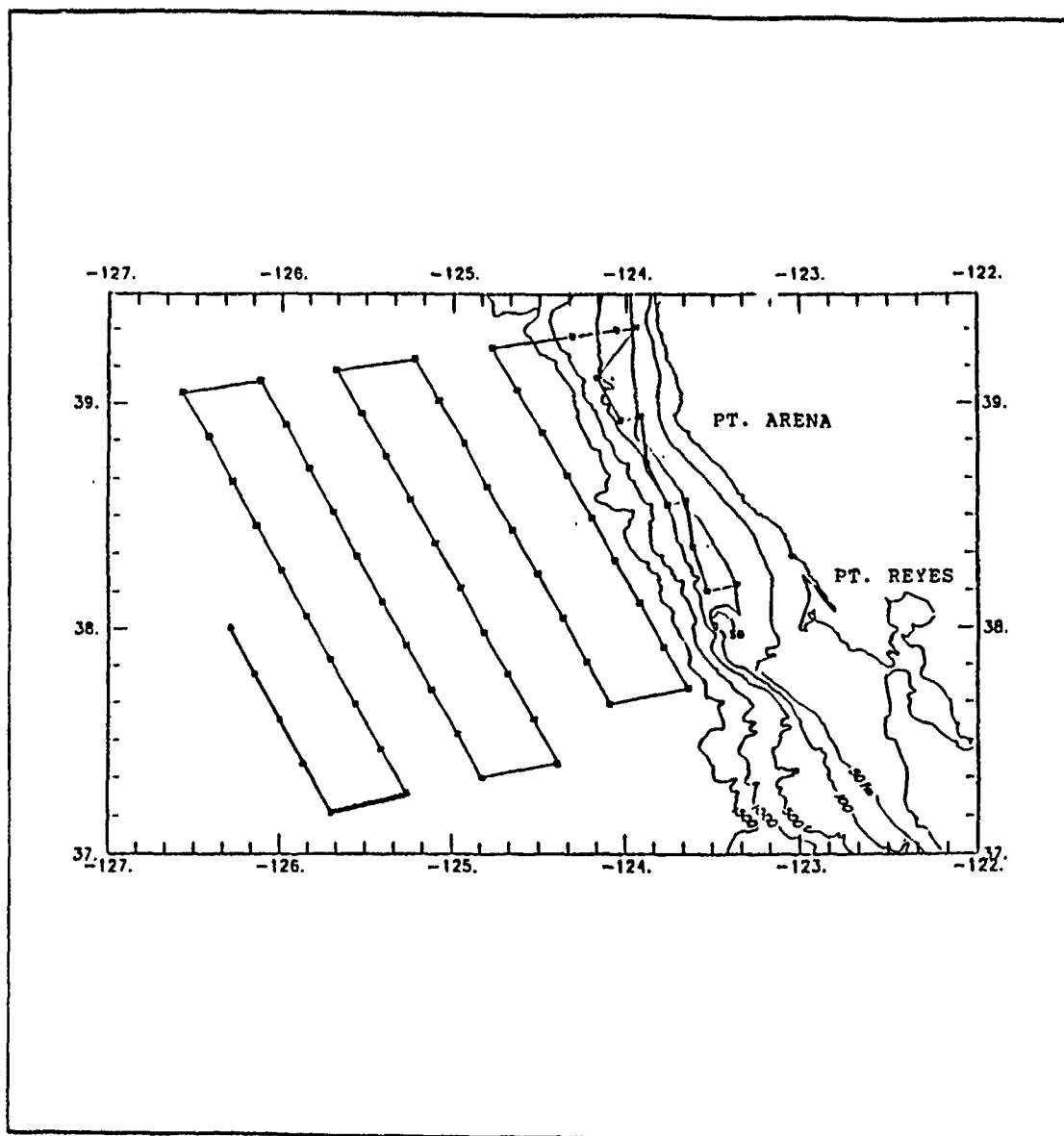
Figure 1. **CTZ Station Grid for 1988:** The irregular alongshore leg paralleling the coast is leg A, followed by legs B, C, D, E, F, and G. Stations are numbered from the top to the bottom of each leg. Leg A has 12 stations, legs B and C have nine stations each, legs D, E, and F have ten stations each, and leg G has five stations (6 to 10) (from Huyer *et al.*, 1990).

5

CHART OF MODEL DOMAIN AND INCLUDED STATIONS
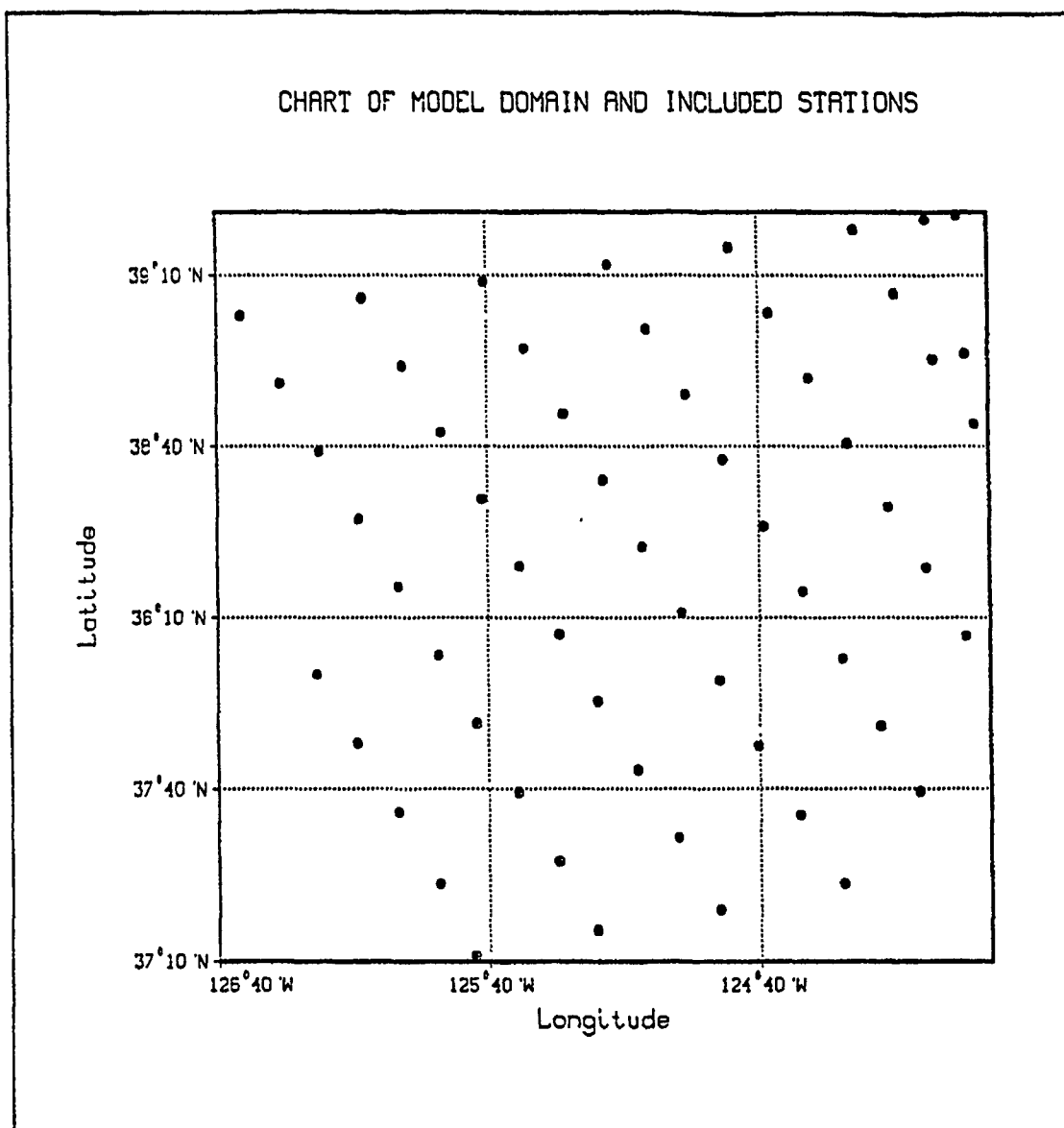
Figure 2.   Chart of Model Domain with Included Stations: Starting from left to right, the alongshore sections are G, F, E, D, C, B, and A. Stations A1 A2, A3, A4, A5, B8 and B9 are excluded from the model domain.
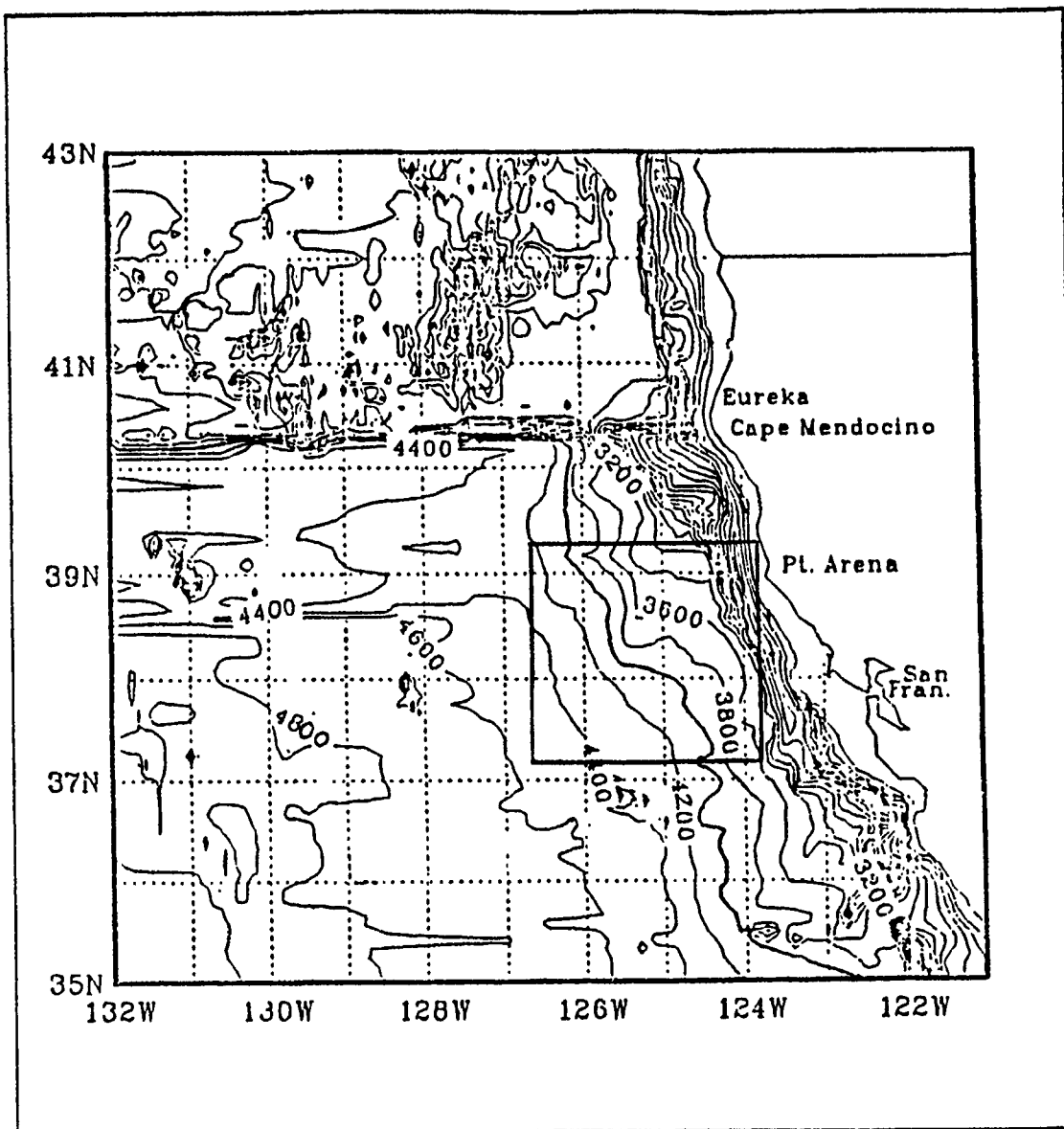
Figure 3.   Actual Topography in the Model Domain: The box shows the area of
the ocean off Point Arena in the model domain. Depths are in meters.

7

III. DATA ACQUISITION AND PROCESSING

A. FIELD ACQUISITION

The three Naval Postgraduate School cruises were CTZR1 (6 to 12 July 1988), CTZR2 (13 to 18 July 1988), and CTZ2 (22 to 26 July 1988), all aboard R/V POINT SUR. Both acoustic doppler current profiler (ADCP) data and conductivity, temperature and depth (CTD) data were acquired. This study will concentrate predominantly on the results from cruise CTZR1.

CTD measurements onboard R/V POINT SUR were made with an NBIS CTD system. Temperature measurement accuracy was better than ± 0.01 C and salinity measurement accuracy was about ± 0.003 psu. An ADCP made by RD Instruments was operated continuously onboard R/V POINT SUR. The transducer operated at 150 kHz with a 4 meter pulse length and a nominal range of 350 meters. Returning echoes were sampled selectively in 4 meter bins to produce a vertically-averaged, ship-relative velocity. Relative velocity profiles were obtained once every three minutes. Twenty-five meters was the shallowest level to yield reliable data (Huyer et al., 1990).

Figure 4 is an infrared Advanced Very High Resolution Radiometer (AVHRR) image from the National Oceanic and Atmospheric Administration (NOAA) NOAA-9 satellite, taken 09 July 1988 of the ocean off the coast of northern California. Cape Mendocino, Point Arena, and Point Reyes can be seen. The large filament oriented northeast to southwest off of Point Arena is the filament under study.

An infrared image of the same area seven days later, taken during the middle of cruise CTZR2, is shown in Figure 5.

Two color-enhanced images of the ocean off Point Arena are shown in Figure 6 and Figure 7. These two images were taken before and after cruise CTZ2.

The four images show the spatial and temporal evolution of the complex sea surface temperature field. The prevailing northwesterly winds in the summer cause Ekman transport of coastal waters offshore, which induces the upwelling of cooler subsurface water. This cool subsurface upwelled water is indicated by the lighter shades in the black and white images and the blues and purples in the color-enhanced images. Two large meanders of the California Current can be seen in the 09 July, 16 July, and 19 July images, with the filament under study separating the two meanders. In the black and white images, eddy-like features can be seen offshore south of Cape Mendocino, Point Arena,
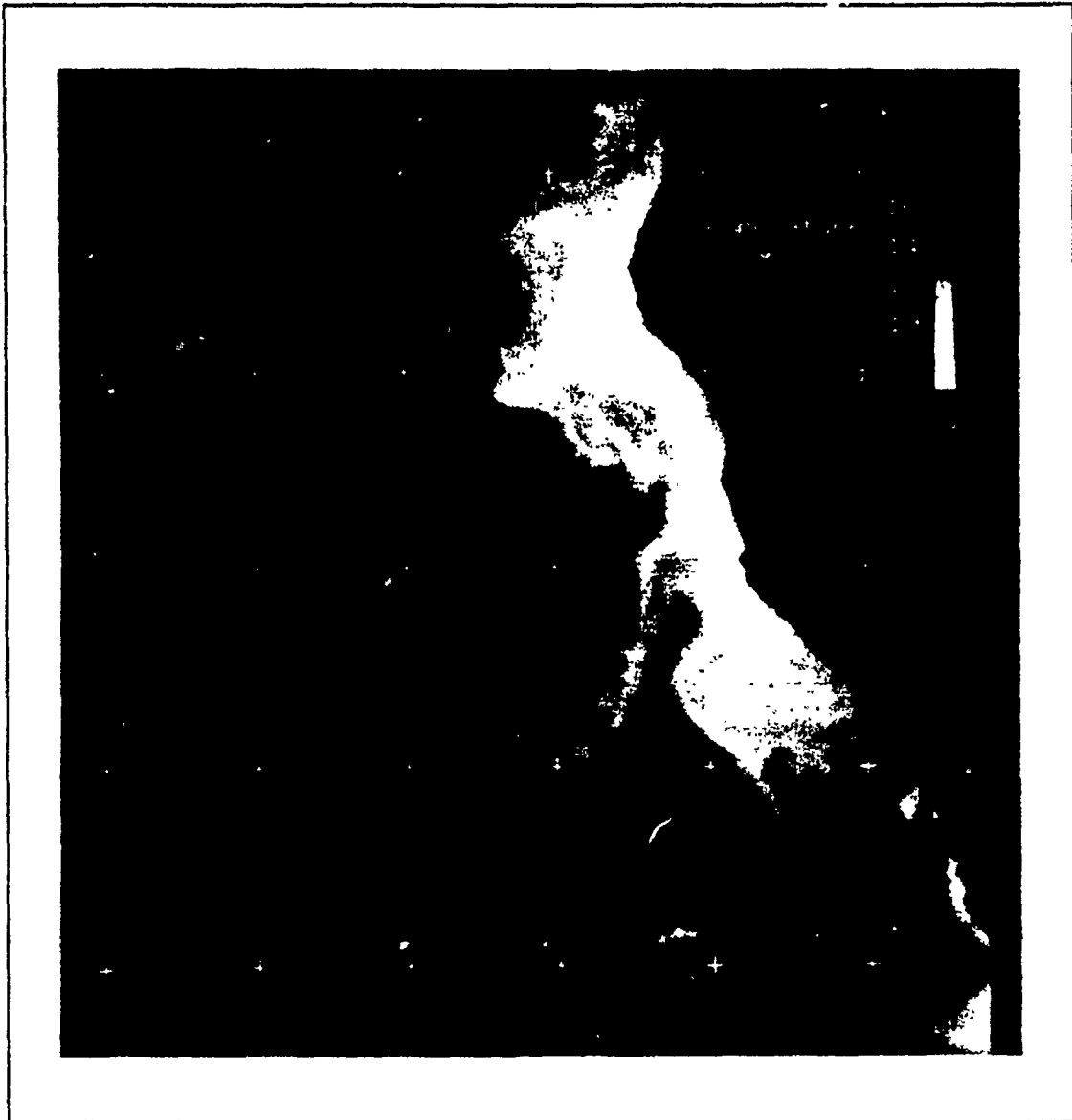
Figure 4.   AVHRR Infrared Image of the Ocean Off the Coast of Northern
California, 09 July 1988:   Darker shades denote warmer temperatures.
Lighter shades denote cooler temperatures.   The latitude coordinates
start at 37˚N at the bottom left corner and increase to 41˚N. The longi-
tude coordinates start at 123˚W at the bottom right corner and increase
to 128˚W. Satellite image provided courtesy of Prof. Steven R. Ramp
and Mr. Paul Jessen, Oceanography Department, Naval Postgraduate
School.

16-Jul-88 1548Z

Figure 5.   AVHRR Infrared Image of the Ocean Off the Coast of Northern California, 16 July 1988:   Darker shades denote warmer temperatures. Lighter shades denote cooler temperatures.   The latitude coordinates start at 37˚N at the bottom left corner and increase to 41˚N. The longitude coordinates start at 123˚W at the bottom right corner and increase to 125 W.   Satellite image provided courtesy of Prof. Steven R. Ramp and Mr. Paul Jessen, Oceanography Department, Naval Postgraduate School.

Figure 6.   Color-Enhanced AVHRR Infrared Image of the Ocean Off the Coast of Northern California, 19 July 1988:   Purples and blues denote cooler temperatures. Violets and reds denote warmer temperatures. Satellite image provided courtesy of Prof. Timothy P. Stanton and Mr. James Stockel, Oceanography Department, Naval Postgraduate School.

and Point Reyes. These satellite images help to give an appreciation of the complex way in which the California Current interacts with the coastal waters to produce the filaments and eddies evident in these images.

11
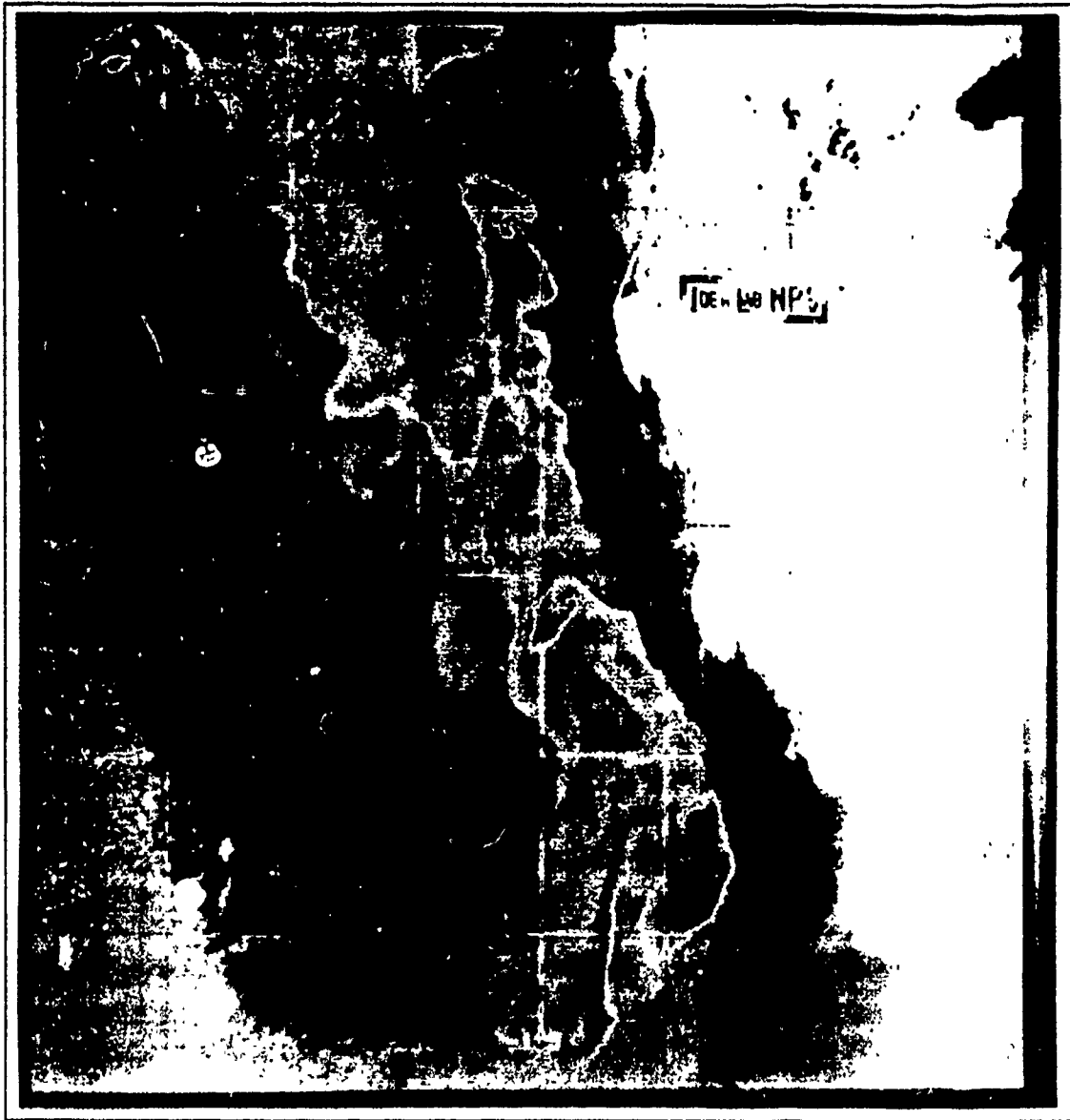
Figure 7.   Color-Enhanced AVHRR Infrared Image of the Ocean Off the Coast of
Northern California. 27 July 1988:   Purples and blues denote cooler
temperatures. Violets and reds denote warmer temperatures. Satellite
image provided courtesy of Prof. Timothy P. Stanton and Mr. James
Stockel, Oceanography Department, Naval Postgraduate School.

B. DATA PROCESSING

The acquired temperature data was objectively analyzed using optimum interpo-
lation as first detailed by Gandin (1965) for meteorological use and later applied to

oceanographic data by Bretherton *et al.,* (1976) and Carter and Robinson (1987). The method has the following features (Stanton and Stockel, 1988):

Provides a consistent method to represent sparsely sampled fields;

Forms an optimal estimate of an n-dimensional variable at gridded intervals based on a measured and/or modeled correlation function;

Provides a measure of the error of the estimated variable at each grid point;

Allows straightforward interfacing to models and calculations involving field differences and integration, and 'standardizes' criteria for graphical representation of mapped data fields.

Processing the acquired data for initialization of the 20-level model, which carries only temperature as a scalar, proceeded as follows. The mean temperature and mean salinity profiles for each of the three cruises was calculated. The acquired temperature data, $T(z)$, was used with the domain mean salinity profile, $\bar{S}(z)$, in an iterative scheme to produce an apparent temperature profile, $T_a(z)$, for input into the model. The full equation of state was used in the iterative scheme to derive $T_a(z)$. The density calculated from the apparent temperature and domain mean salinity, $\rho(T_a(z), \bar{S}(z))$, was the same as the *in situ* density, $\rho(T(z), S(z))$, measured at each station. The apparent temperatures were vertically averaged in four-meter bins at 5 m, 25 m, 65 m, 125 m, 205 m, 305 m, and 425 m (the first seven k-levels in the model) in the optimum interpolation program for cruises CTZR1 and CTZ2. The apparent temperatures were vertically averaged in four-meter bins at 5 m, 25 m, 65 m, 125 m, and 205 m for cruise CTZR2.

The spatial m an temperature profile was extended to 4000 m by fitting an exponential tail to the last two points of the calculated mean temperature profile. This extended mean temperature profile was used to calculate the first three dynamical vertical modes $T_1(k)$, $T_2(k)$, and $T_3(k)$ for temperature. The objective was to extrapolate the perturbation temperature down to 4000 m using modal profiles with weights determined according to how well the data in the upper 425 m (205 m for CTZR2) fit the respective mode. The procedure, as outlined below, is described in detail in Rienecker *et al.,* (1987).

The initial assumption made was that

$$T'(i,j,k) = T(i,j,k) - \bar{T}(k), \qquad \{1\}$$

i, j, k, are the gridpoint indices for the x, y, and z directions, respectively,

$T'(i,j,k)$ is the perturbation part of the temperature at the gridpoint,

13

$T(i,j,k)$ is the objectively analyzed temperature at the gridpoint, and

$\overline{T}(k)$ is the mean temperature at level k.

The perturbation temperature $T'(i,j,k)$ is assumed to be a linear combination of the first three dynamical vertical modes, such that

$$T'(i,j,k) = a_1(i,j)T_1(k) + a_2(i,j)T_2(k) + a_3(i,j)T_3(k), \qquad \{2\}$$

$a_1 = a_1(i,j)$ is the weighting given to $T_1(k)$,

$a_2 = a_2(i,j)$ is the weighting given to $T_2(k)$, and

$a_3 = a_3(i,j)$ is the weighting given to $T_3(k)$.

Solutions for a_1, a_2, and a_3 are desired.

Four equations are derived from equation $\{2\}$:

$$<T'(i,j,k)> = a_1 <T_1(k)> + a_2 <T_2(k)> + a_3 <T_3(k)>, \qquad \{3\}$$

$$<T_1(k)T'(i,j,k)> = a_1 <T_1(k)T_1(k)> + a_2 <T_1(k)T_2(k)> + a_3 <T_1(k)T_3(k)>, \quad \{4\}$$

$$<T_2(k)T'(i,j,k)> = a_1 <T_2(k)T_1(k)> + a_2 <T_2(k)T_2(k)> + a_3 <T_2(k)T_3(k)>, \quad \{5\}$$

$$<T_3(k)T'(i,j,k)> = a_1 <T_3(k)T_1(k)> + a_2 <T_3(k)T_2(k)> + a_3 <T_3(k)T_3(k)>, \quad \{6\}$$

and define the bracketed terms, $<Q> \equiv \sum_1^7 Q\Delta z(k)/\sum_1^7 \Delta z(k)$, where $\Delta z(k)$ is the vertical difference between adjacent k levels in the model. Thus, $<Q>$ is the vertical average of Q over the top seven levels of the model which contain all the analyzed observations.

The system of four equations in three unknowns (a_1, a_2, a_3) can be solved by linear least squares methods. After a_1, a_2, and a_3 are found for each point in the domain of the model, equation $\{2\}$ can then be used to find $T'(i,j,k)$ for k = 8 to k = 20. For CTZR2, the procedure is similar, except only five levels of data are available, and the extrapolation is used to define $T'(i,j,k)$ for k = 6 to k = 20.

Solutions to equations $\{3\}$ through $\{6\}$ above yielded values of a_1 which produced negative temperatures for $T(i,j,k)$ at k levels 9 through 14 (725 m to 1825 m), which caused the model to become unstable at 42 time steps (0.29 day). Apparently, the CTD casts to only 500 meters were not sufficient to adequately define the first dynamical mode to 4000 m. Accordingly, the new system of equations used to solve for a_2 and a_3 were the following:

$$<T'(i,j,k)> = a_2 <T_2(k)> + a_3 <T_3(k)>, \qquad \{7\}$$

$$< T_1(k)T'(i,j,k)> = a_2 < T_1(k)T_2(k)> + a_3 < T_1(k)T_3(k)>, \qquad \{8\}$$

$$< T_2(k)T'(i,j,k)> = a_2 < T_2(k)T_2(k)> + a_3 < T_2(k)T_3(k)>, \qquad \{9\}$$

$$< T_3(k)T'(i,j,k)> = a_2 < T_3(k)T_2(k)> + a_3 < T_3(k)T_3(k)>. \qquad \{10\}$$

The resulting solutions for a_2 and a_3 provided positive extrapolated temperatures in the model domain; however, horizontal temperature fluctuations on scales less than the observation scale (about 25 km) were apparently introduced during the objective analysis scheme. This was discovered after contouring the extrapolated input temperatures as seen in Figure 8.

If these small scales are in fact physical, then their vertical scales should also be small (much smaller than that of dynamical modes 2 and 3). Since the extrapolation scheme uses modes 2 and 3 to extrapolate the perturbation temperatures down to 4000 m, the assumption is that the horizontal scales are those of the deep modes, which are larger than 25 km. Thus the $T'(i,j,k)$ fields were smoothed to eliminate the small scales. The following smoother was used:

$$T^s = \frac{1}{12}(4T_0 + T^+ + T^x), \qquad \{11\}$$

$T_0 = T'(i,j,k)$, the perturbation temperature at each domain gridpoint,

$T^- = T'(i+1,j,k) + T'(i-1,j,k) + T'(i,j+1,k) + T'(i,j-1,k)$,

$T^x = T'(i+1,j+1,k) + T'(i-1,j+1,k) + T'(i-1,j-1,k) + T'(i+1,j-1,k)$,

and smoothing was accomplished by setting $T'(i,j,k) \equiv T^s$ (double smoothing). An example of the resulting smoothed field is shown in Figure 9.

An example of the extrapolation of the apparent temperature to deep depths is now given. Two points from the CTZR1 five meter plot of apparent temperature, (52, 16) and (248, 220), will be used as examples.

Point (52, 16) is in a warm region located in the southwestern corner of the grid. Point (248, 220) is in a cold eddy feature in the northeastern corner of the grid, off Point Arena. The locations of the two points are shown in Figure 10.

The modal temperature values for CTZR1 are shown in Figure 11. The third mode has the highest amplitude (about 44°C) followed by the second mode (maximum amplitude about 18°C) and the first mode (maximum amplitude about 3°C). The first zero

15

PLOT OF APPARENT TEMPERATURE
AT DEPTH OF 565 METERS
CRUISE CTZR1
06-12 JULY 88
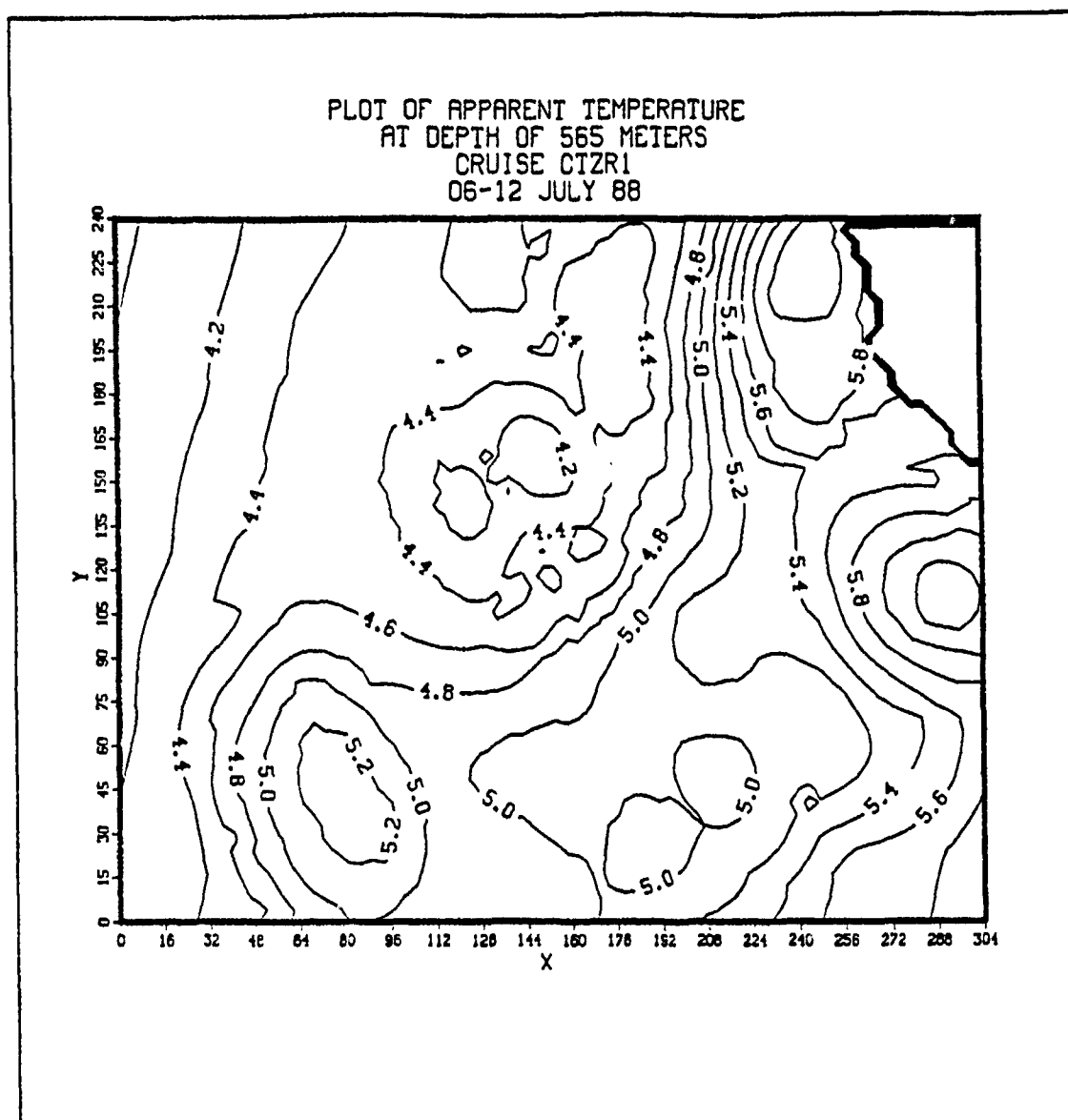
Figure 8.   Contour Plot of Extrapolated Apparent Temperature at 565 m (un-smoothed):   The numerals on the abscissa and ordinate refer to dis-tances in kilometers. The model domain only includes the i indices from 0 to 256 and the j indices from 1 to 240. The irregular contours in the northeast corner are the zero contours which designate the coastline (Point Arena is outlined).

crossing of the third mode is at about 425 m and the second zero crossing is at about 1250 m. The zero crossing of the second mode is at about 800 m.

16

PLOT OF APPARENT TEMPERATURE
AT DEPTH OF 565 METERS
CRUISE CTZR1
06-12 JULY 88
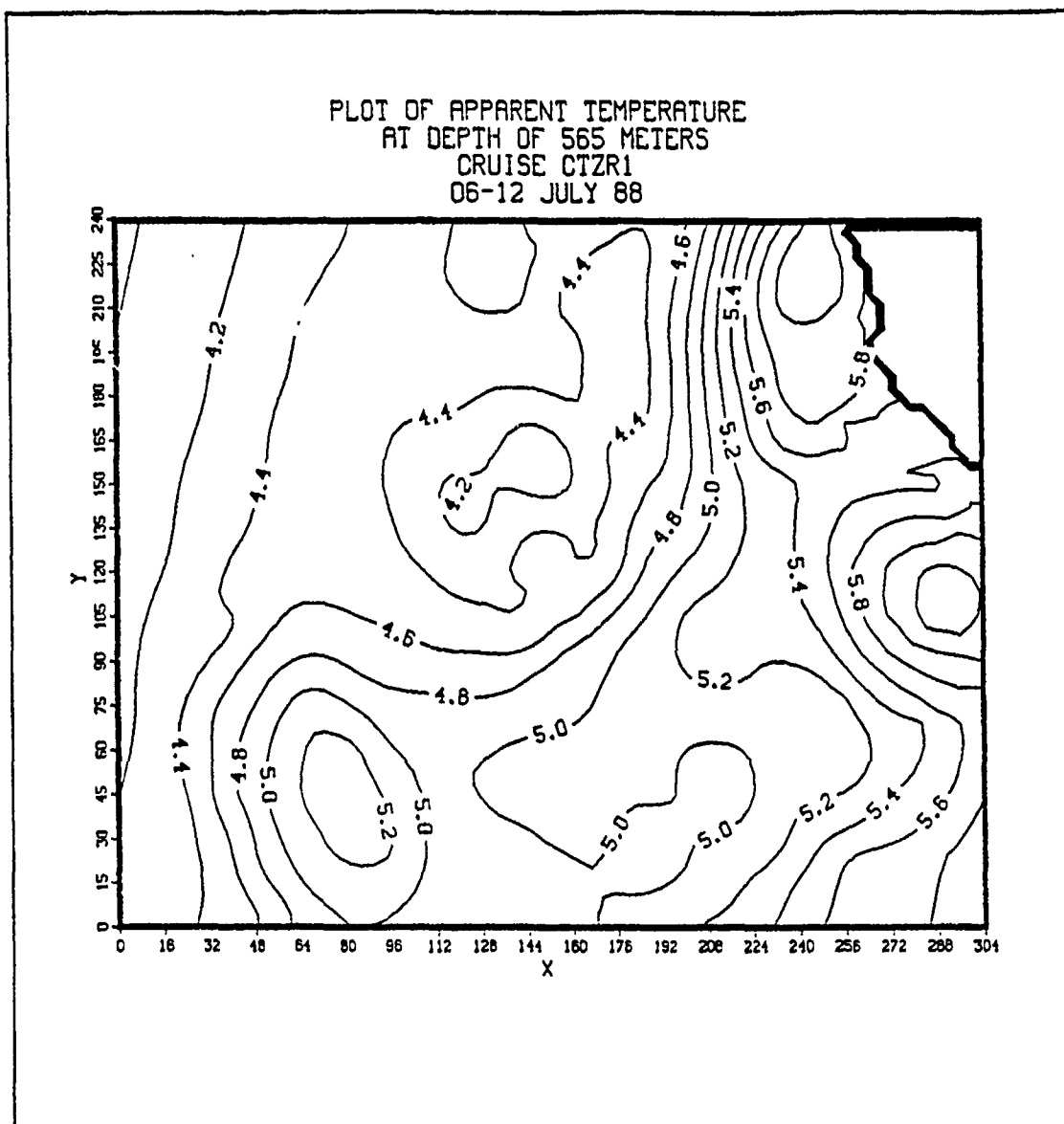
Figure 9.   Contour of Extrapolated Apparent Temperature at 565 m (smoothed): The numerals on the abscissa and ordinate refer to distances in kilometers. The model domain only includes the i indices from 0 to 256 and the j indices from 0 to 240. The irregular contours in the northeast corner are the zero contours which designate the coastline (Point Arena is outlineᴜ).

The plots of the a_2 and a_3 values for cruise CTZR1 are shown in Figure 12 and Figure 13, respectively. The fields are clearly related to the synoptic scale temperature patterns shown in Figure 8 and Figure 9.
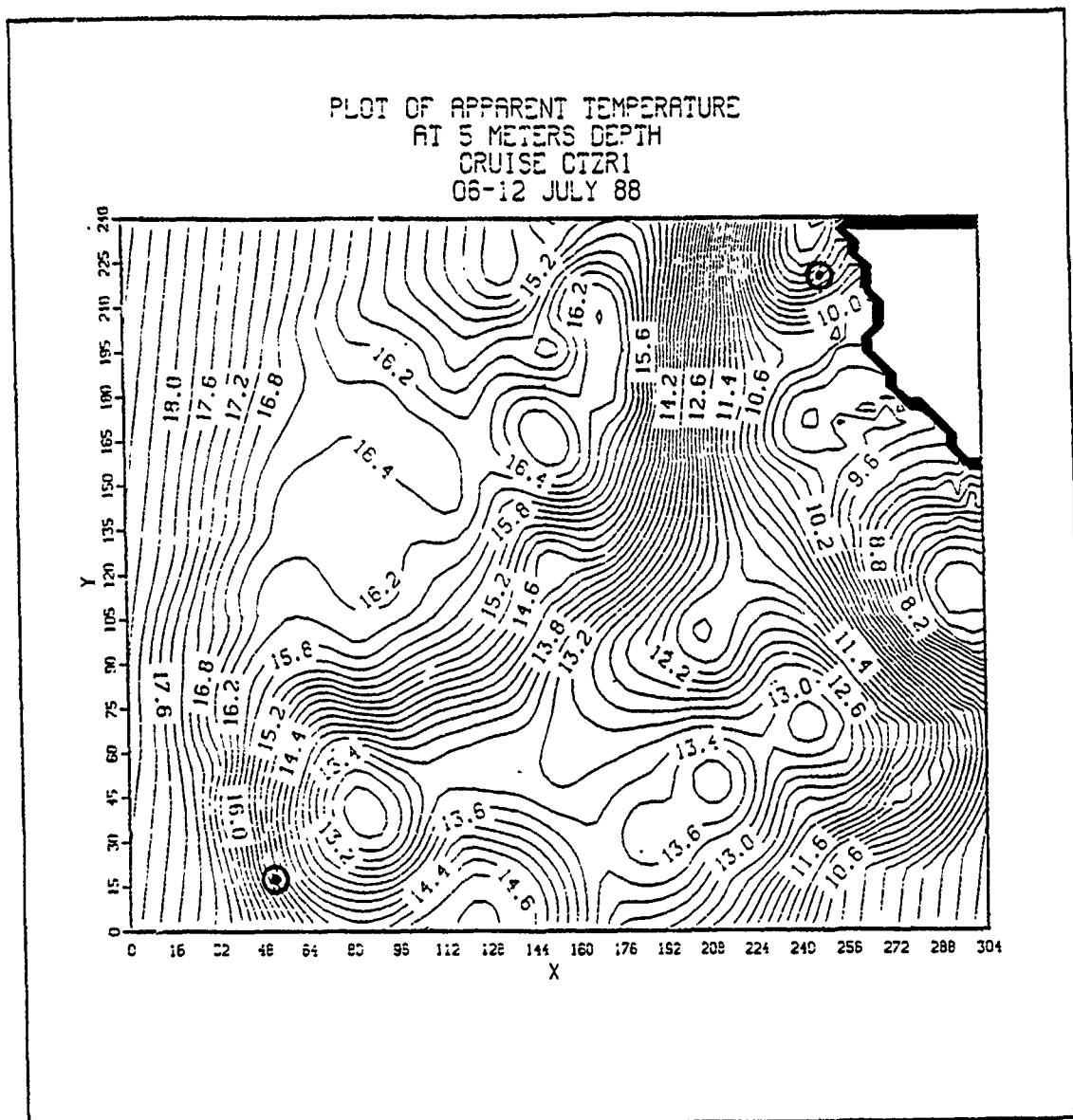
Figure 10. Plot of Apparent Temperature at Five Meters Depth, Cruise CTZR1, 06-12 July 1988: The heavily outlined area in the northeast corner is the coastline. The two points of interest are marked with bullseyes. The model domain only includes the area from x = 0 to x = 256 km and y = 0 to y = 240 km.

Note that for point (52, 16), the a_3 value is positive and the a_2 value is negative, with $|a_3| > |a_2|$. This implies that the perturbation temperature at (52, 16) is strongly influenced by the third mode and will be positive until the first zero crossing of mode three. After the first zero crossing, the perturbation temperature values will be negative until

18
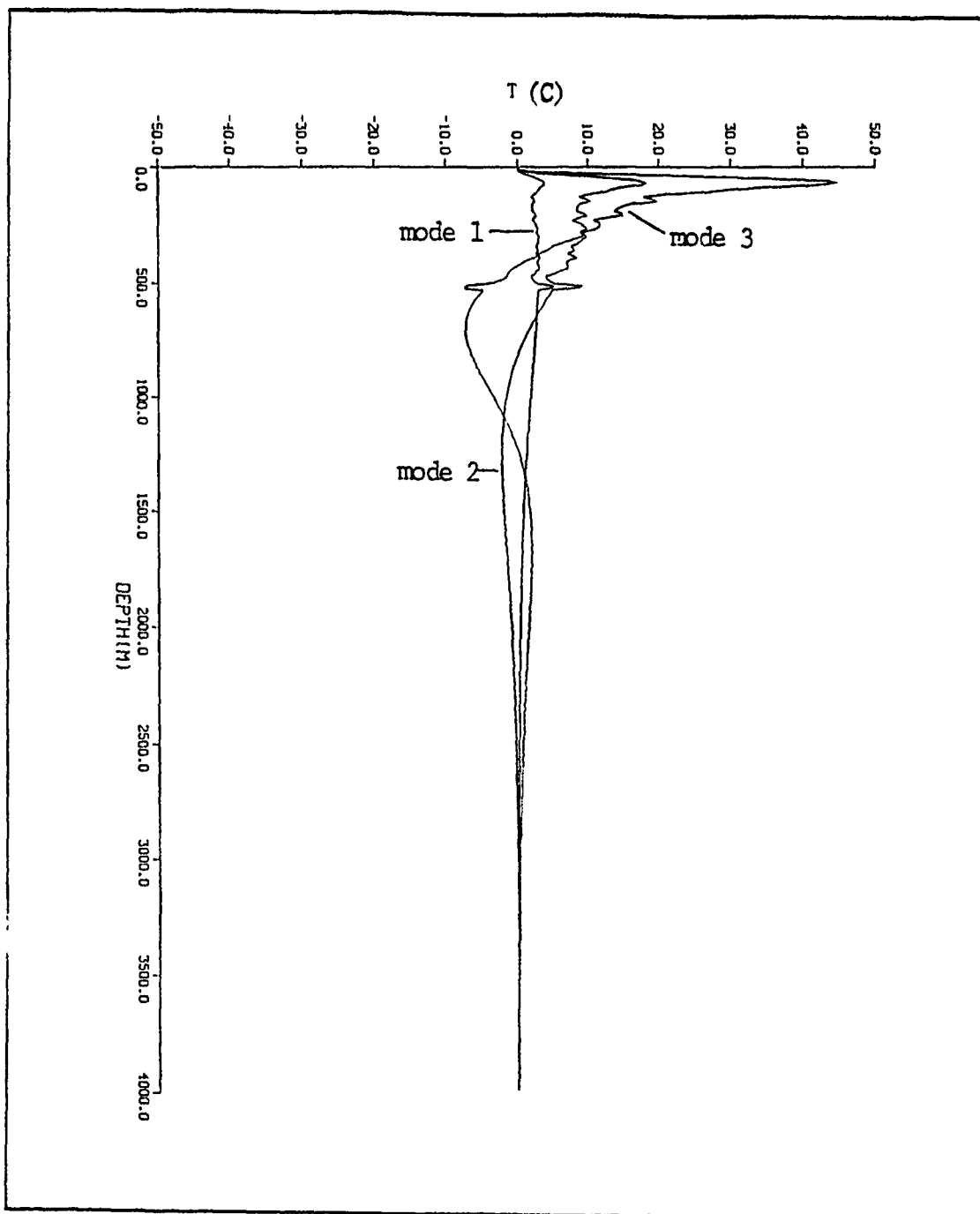
Figure 11. First Three Modes of Temperature (C) for Cruise CTZR1

the second zero crossing. After the second zero crossing, the perturbation temperatures will be positive to 4000 m.
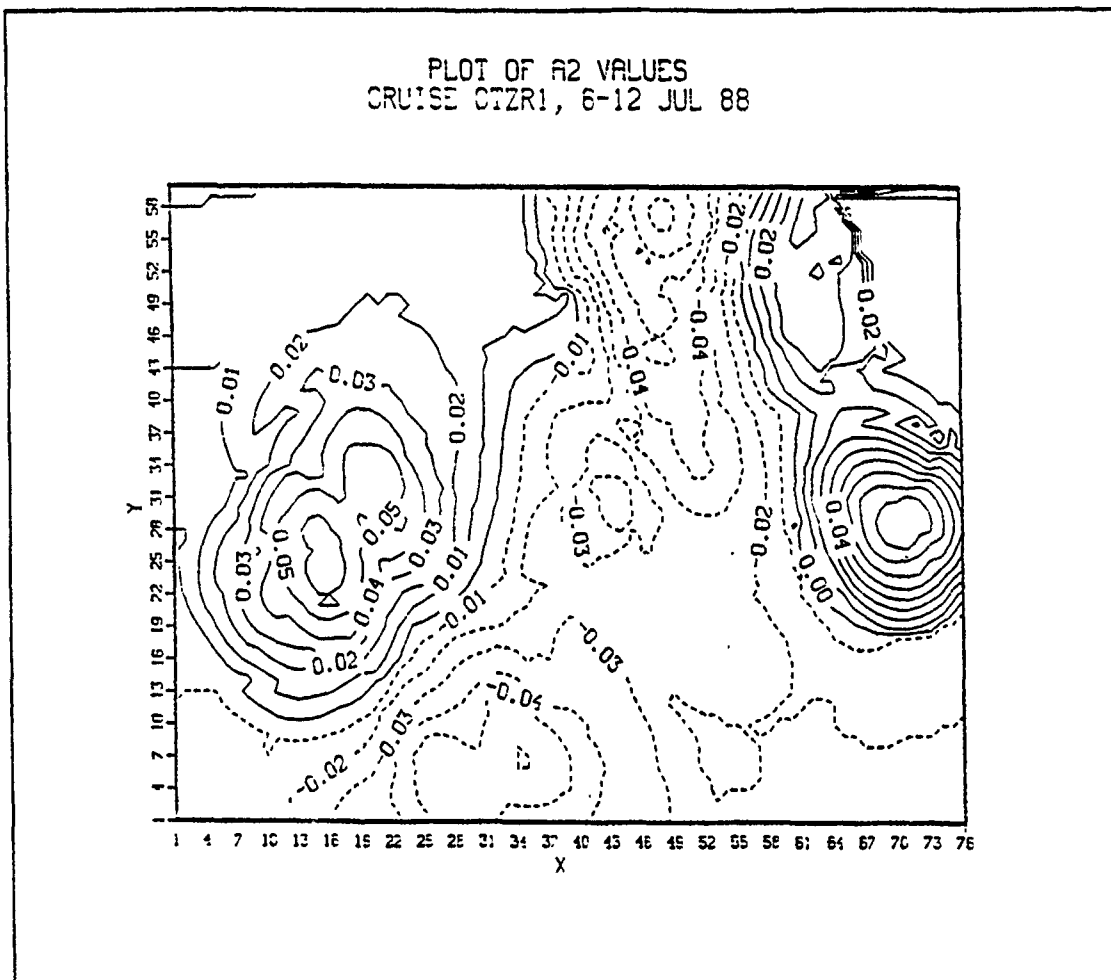
Figure 12.   Plot of A2 Values, Cruise CTZR1, 06-12 July 1988

For point (248, 220), the a_3 value is negative and the a_2 value is positive, with $|a_3| > |a_2|$. This implies that the perturbation temperatures at (248, 220) will be negative until the first zero crossing of the third mode, positive until the second zero crossing, and negative to 4000 m after the second zero crossing.

The plot of perturbation apparent temperature versus depth for point (52, 16) is given in Figure 14. The plot of perturbation apparent temperature versus depth for point (248, 220) is given in Figure 15. Total and mean apparent temperature profiles for points (52, 16) and (248, 220) are plotted in Figure 16 and Figure 17.

The point (248, 220) is an example of a location where the objective analysis resulted in a hydrostatically unstable profile of apparent temperature. Any hydrostatic instability was dealt with by subjecting the respective point to a convective adjustment which cor-

Figure 13.   Plot of A3 Values, Cruise CTZR1, 06-12 July 1988

rected the instability.   The result of this convective adjustment for point (248, 220) is shown in Figure 18.   The temperature profile is now hydrostatically stable.   Together, these figures show that the vertical extrapolation procedure was effective in extending the perturbation temperatures to 4000 m.

The need for a convective adjustment for some of the data points is attributable to the correlation function used in the objective analysis scheme.   The correlation function is an even, smooth, monotonic function with a zero crossing in the horizontal space dimension modeled from observed data.   An instability in an objectively analyzed profile can occur if the correlation function encounters a quickly changing monotonic profile in the negative portion of the correlation function.   The large negative contribution created by the product of the correlation function and the value of the profile at a spe-
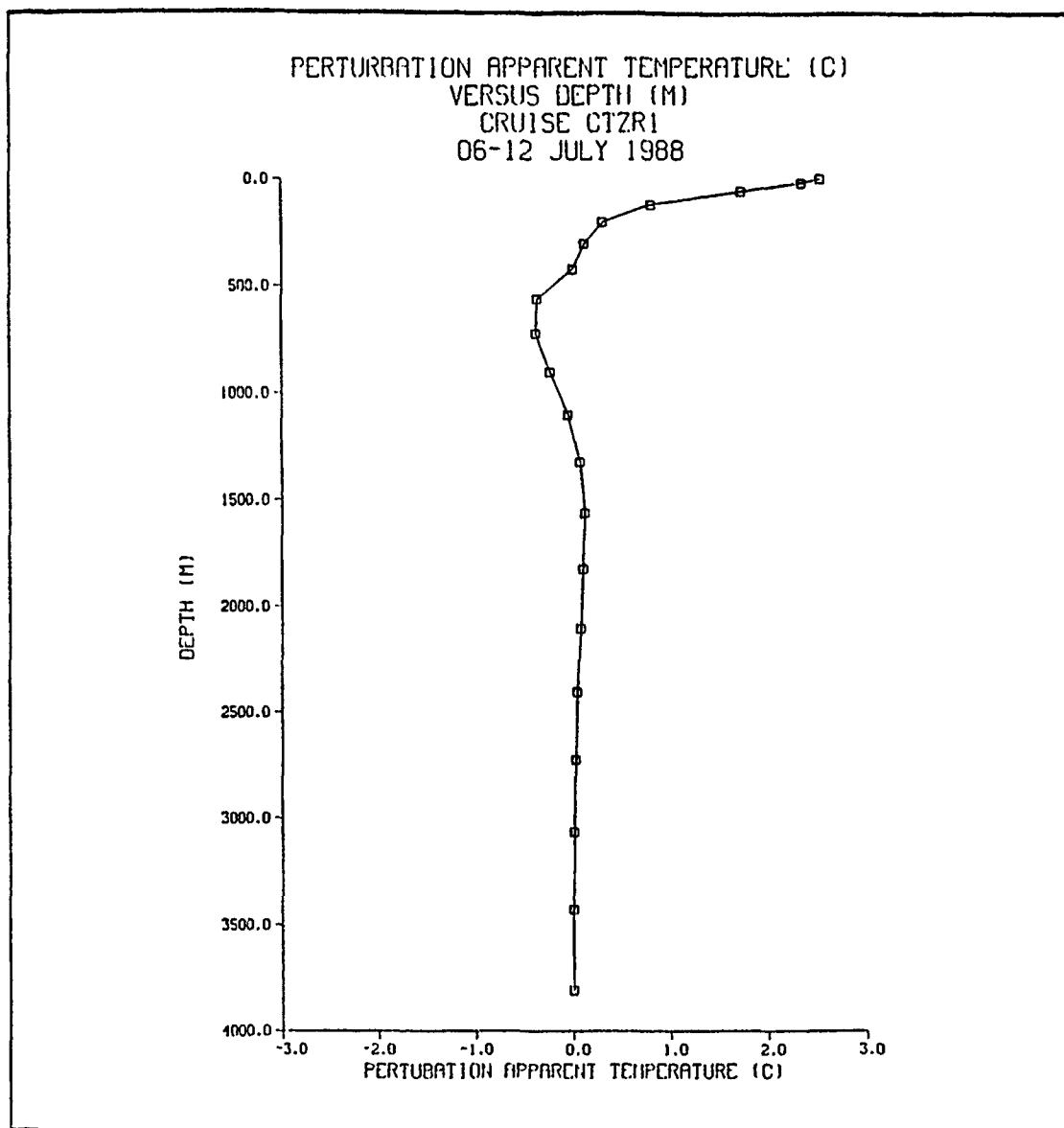
Figure 14. Perturbation Apparent Temperature Versus Depth for Point (52, 16)

cific depth may be enough to cause the once stable profile to develop spurious hydrostatic instability. For cruise CTZR1, a plot of the points requiring a convective adjustment is given in Figure 19. Most of the convective adjustment occurred north and south of the jet. Cruise CTZR2 required convective adjustment at all data points. Cruise CTZ2 required convective adjustment on either side of the jet (the jet had reoriented itself from a northeast-southwest direction to a nearly north-south direction) as
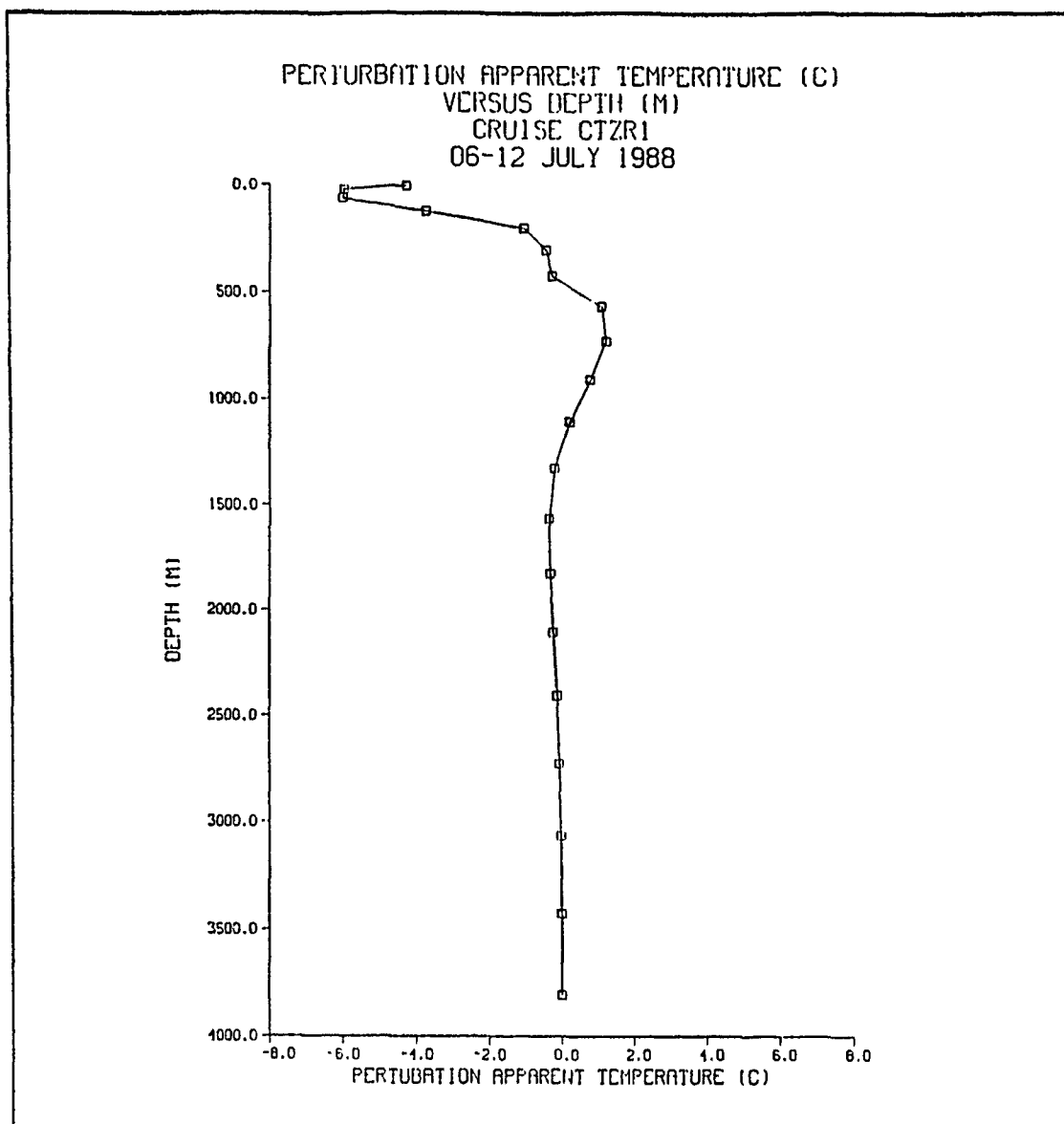
Figure 15. Perturbation Apparent Temperature versus Depth for Point (248, 220)

seen in Figure 20. The convective adjustment at point (248, 220) for both CTZR2 and CTZ2 are shown in Figure 21 and Figure 22.

23

**TOTAL AND
MEAN APPARENT TEMPERATURE (C)
VERSUS DEPTH (M)
CRUISE CTZR1
06-12 JULY 1988**
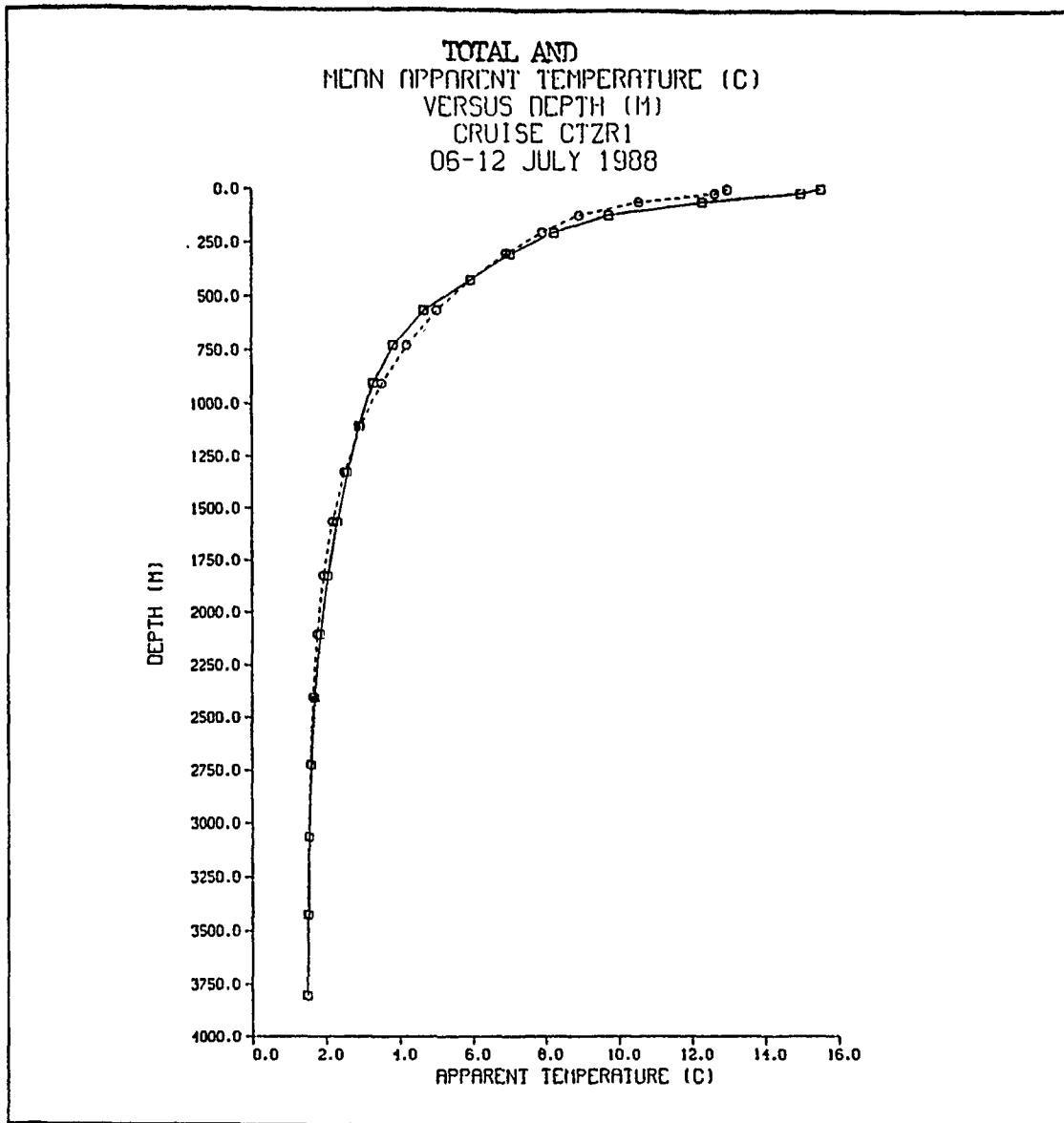
Figure 16.   Plot of Total and Mean Apparent Temperature for Point (52, 16):   Total apparent temperature is plotted using squares and a solid line. Mean apparent temperature is plotted using circles and a dashed line. The squares and circles are plotted at the k-level depths of the model.
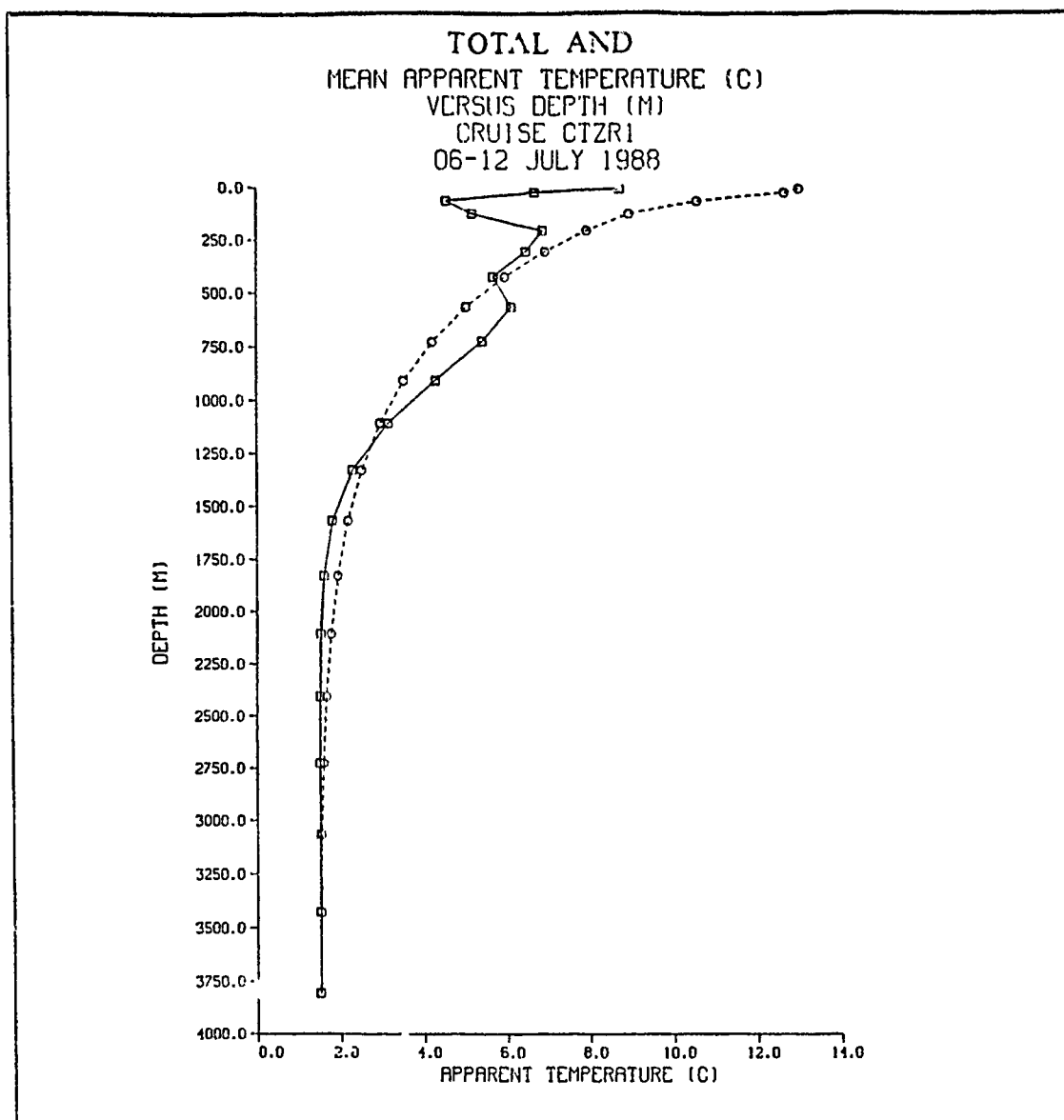
Figure 17. Plot of Total and Mean Apparent Temperature for Point (248, 220): Total apparent temperature is plotted using squares and a solid line. Mean apparent temperature is plotted using circles and a dashed line. The squares and circles are plotted at the k-level depths of the model.

Figure 18. Plot of Total Apparent Temperature for Point (248, 220) after Convective Adjustment, Cruise CTZR1: The solid line and squares denote the hydrostatically unstable profile after extrapolation and before convective adjustment. The dashed line and circles denote the hydrostatically stable profile after convective adjustment.

tadj at day 0 depth 0 ci = 1.00
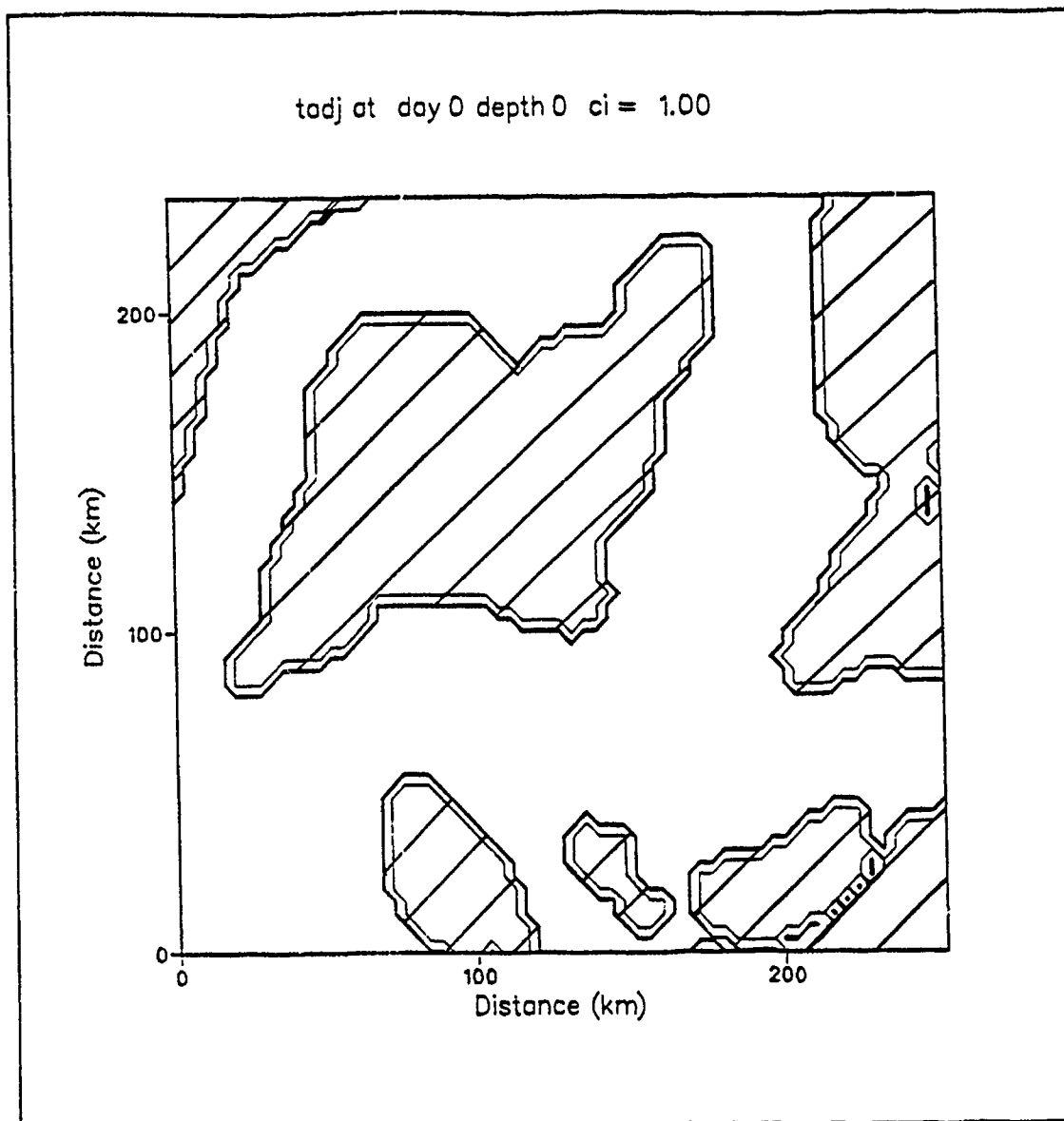
Figure 19. Areas Requiring Convective Adjustment for CTZR1: The hatched areas denote the points which required convective adjustment before initiating the model run.

27

tadj at day 0 depth 0 ci = 1.00
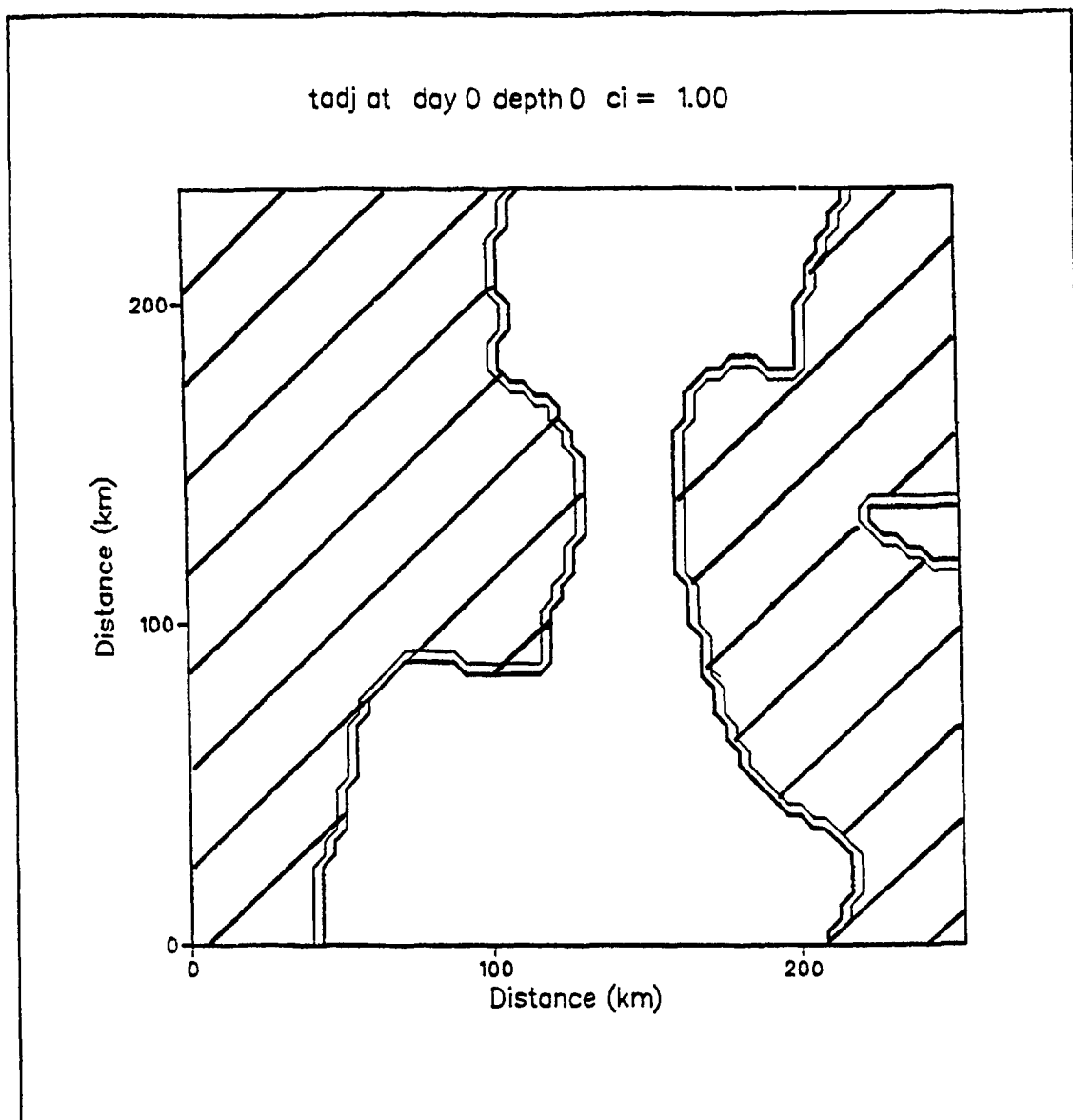
Figure 20. Areas Requiring Convective Adjustment for CTZ2: The hatched areas denote the points which required convective adjustment before initiating the model run.

Total Apparent Temperature (C)
Versus Depth (m)
Cruise CTZR2
13--18 July 1988
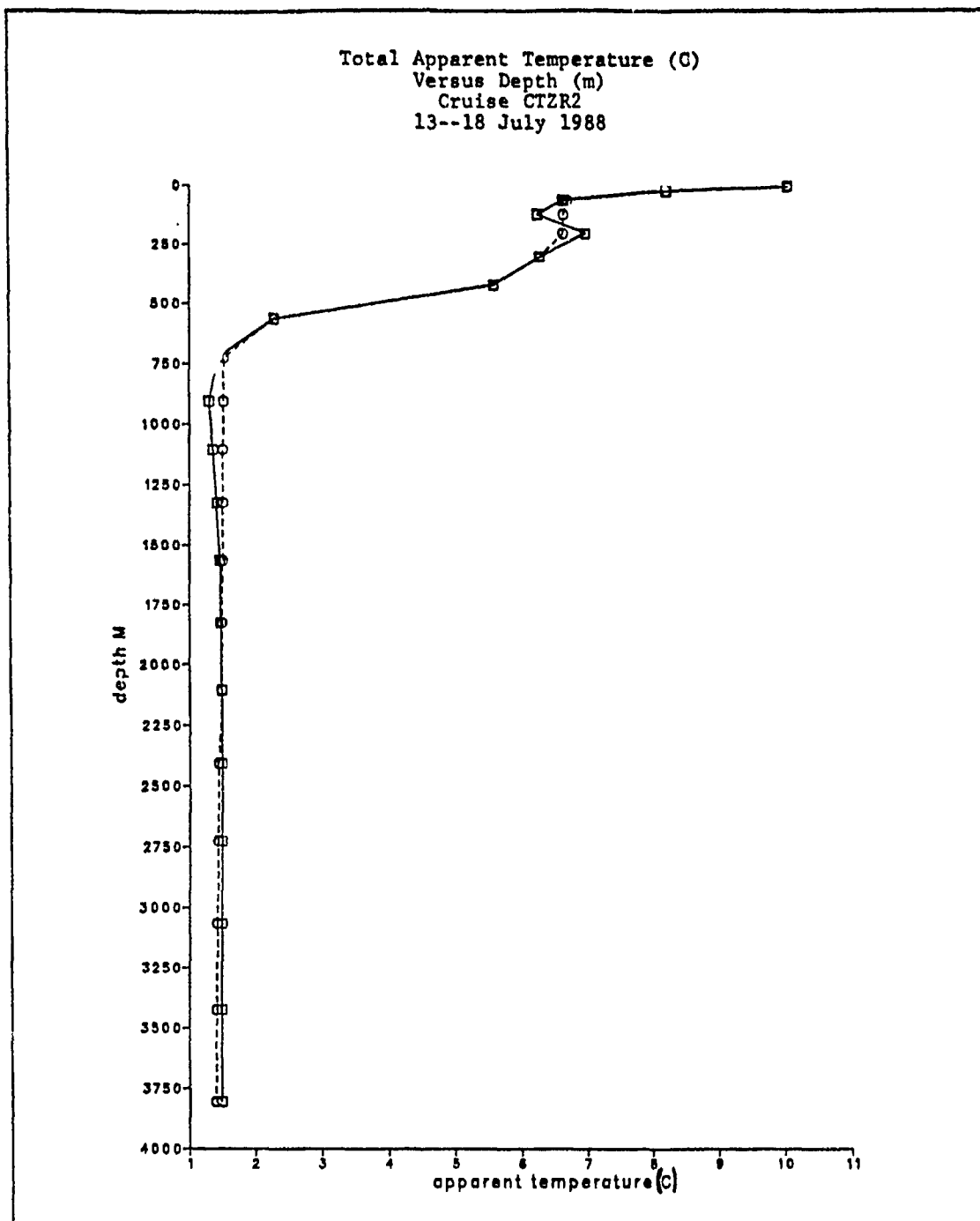
Figure 21.   Plot of Total Apparent Temperature for Point (248, 220) after
Convective Adjustment, Cruise CTZR2:   The solid line and squares
denote the hydrostatically unstable profile after extrapolation and be-
fore convective adjustment.   The dashed line and circles denote the
hydrostatically stable profile after convective adjustment.

29

Total Apparent Temperature (C)
Versus Depth (m)
Cruise CTZ2
22--26 July 1988
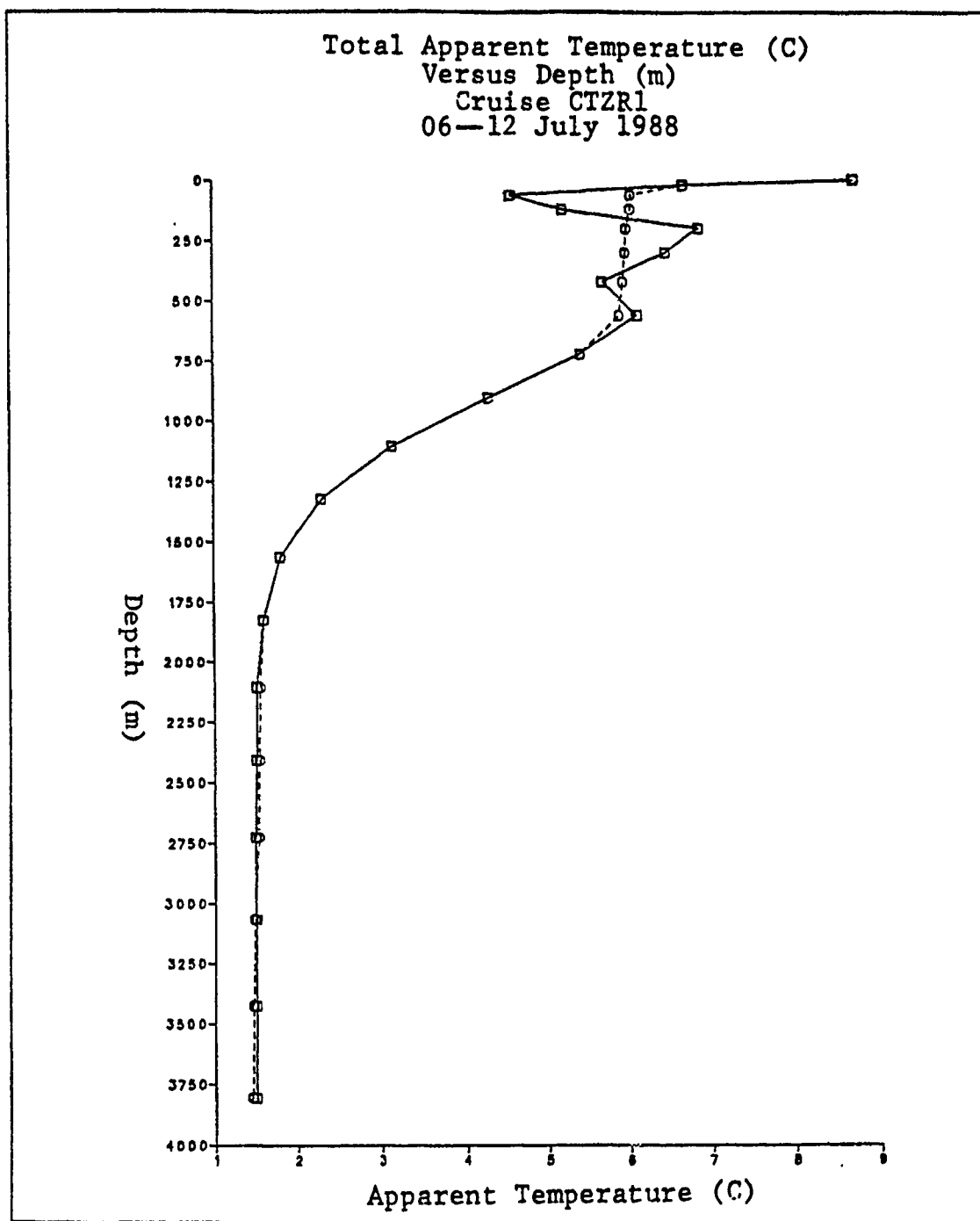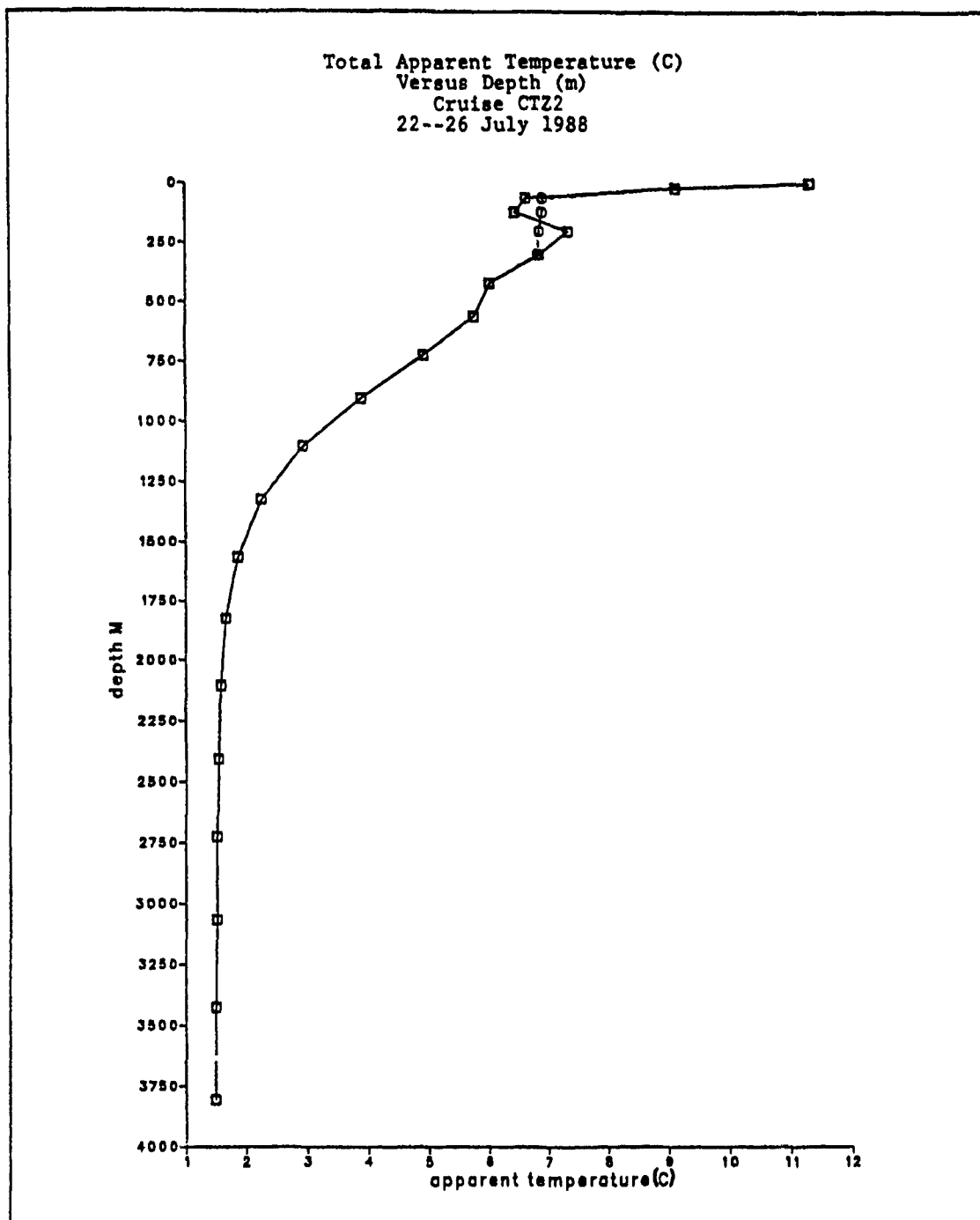
Figure 22.   Plot of Total Apparent Temperature for Point (248, 220) after Convective Adjustment, Cruise CTZ2:   The solid line and squares denote the hydrostatically unstable profile after extrapolation and before convective adjustment.   The dashed line and circles denote the hydrostatically stable profile after convective adjustment.

IV. MODEL RESULTS

The primitive equation model was initialized with the apparent temperature fields described above and geostrophically balanced currents having a zero vertical average. The model was then integrated forward in time for 30 hours ($t \gg f^{-1}$) with the temperature field held fixed. The currents underwent adjustments to a new state of balance in which nonlinearity and eddy diffusion effects are not entirely negligible (as they are in exact geostrophic balance). The resulting density diagnostic currents, which have an important vertical component, are the main subject of analysis and verification.

A. PRESSURE, TEMPERATURE, AND VELOCITY FIELDS

The discussion of model results will be limited to the model output from CTZR1 data and the vertical velocity output at time 30 hours for both CTZR2 and CTZ2 only. Fuller treatment of cruises CTZR2 and CTZ2 are considered to be separate studies.

The apparent temperature fields at 50 m, 100 m, and 200 m at time zero are shown in Figure 23, Figure 24, and Figure 25. Ver ical continuity is evident in the apparent temperature fields. In each level a strong thermal gradient oriented southeast to northwest appears, with a strong jet dividing the domain into two distinct parts. This strong apparent temperature gradient ($\nabla T \approx 1'/8$ km at 50 m and $1'/16$ km at 200 m) is the driving force for the strong initial currents in the upper ocean. These currents are computed from the thermal wind relation and with the assumption that the vertically-averaged current is zero.

The initial u-component and v-component of velocity at 100 meters are shown in Figure 26 and Figure 27. The u-component achieves westward (dashed lines) velocities up to 29 cm sec^{-1} in the southwestern portion of the domain. Weaker eastward flow up to 12 cm sec^{-1} dominates the northern portion of the domain. The v-component achieves southern (dashed lines) speeds up to 25 cm sec^{-1}. Equatorward velocities dominate in the center of the domain. Much weaker poleward velocities up to 7.5 cm sec^{-1} appear in the northwest and southeast quadrants.

After 30 hours, the u-component in the southwestern portion has intensified to greater than 40 cm sec^{-1} (Figure 28). Weaker westward flow greater than 10 cm sec^{-1} is still found in the northern portion of the domain. The v-component has intensified to greater than 30 cm sec^{-1} in the middle and southwestern parts of the domain (Figure 29).

Cruise CTZR1, 06–12 July 1988

T at hour 0, depth 50 m
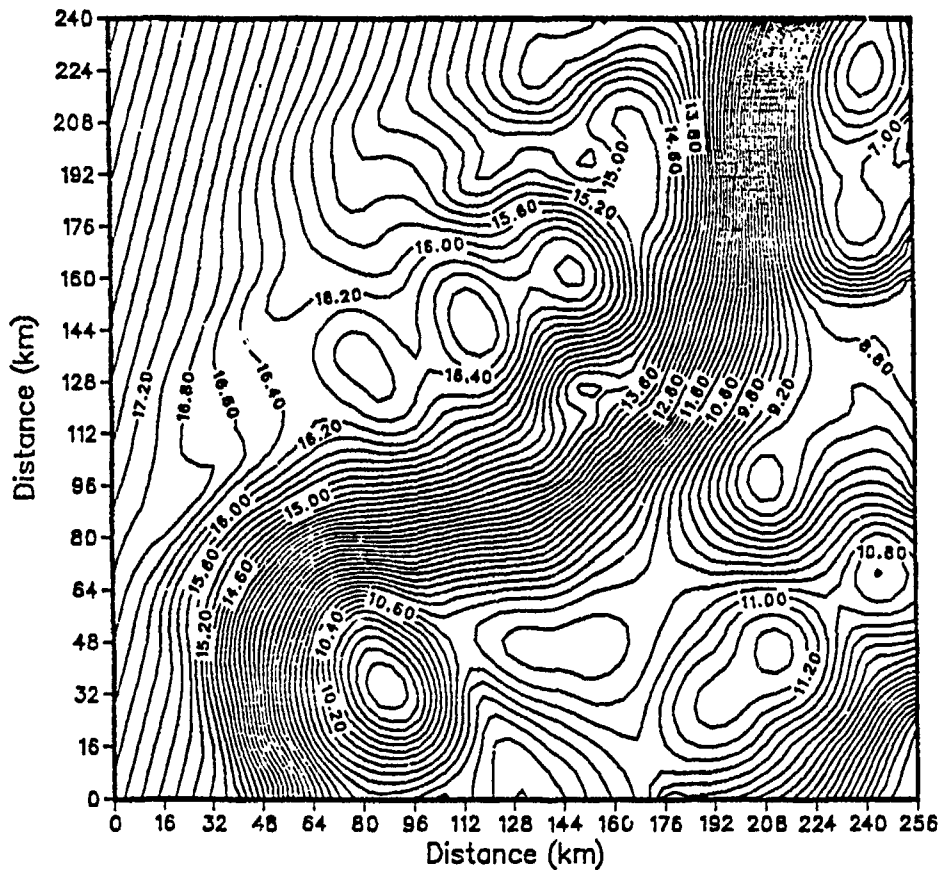
Figure 23. Apparent Temperature at 50 m Depth, Cruise CTZR1: Contour interval is 0.2 C.

The 100 m pressure field (at time zero and at time 30 hr), Figure 30, shows what mechanism can induce a jet. A high pressure center (dynamic height greater than 15 cm) dominates the northwestern portion of the domain, producing anticyclonic flow. The southeastern portion of the domain is dominated by a low pressure center (dynamic height less than -15 cm), producing cyclonic flow. The water between the high and low pressure centers is accelerated between the two pressure extremes which produces the

Cruise CTZR1, 06-12 July 1988

T at hour 0, depth 100 m
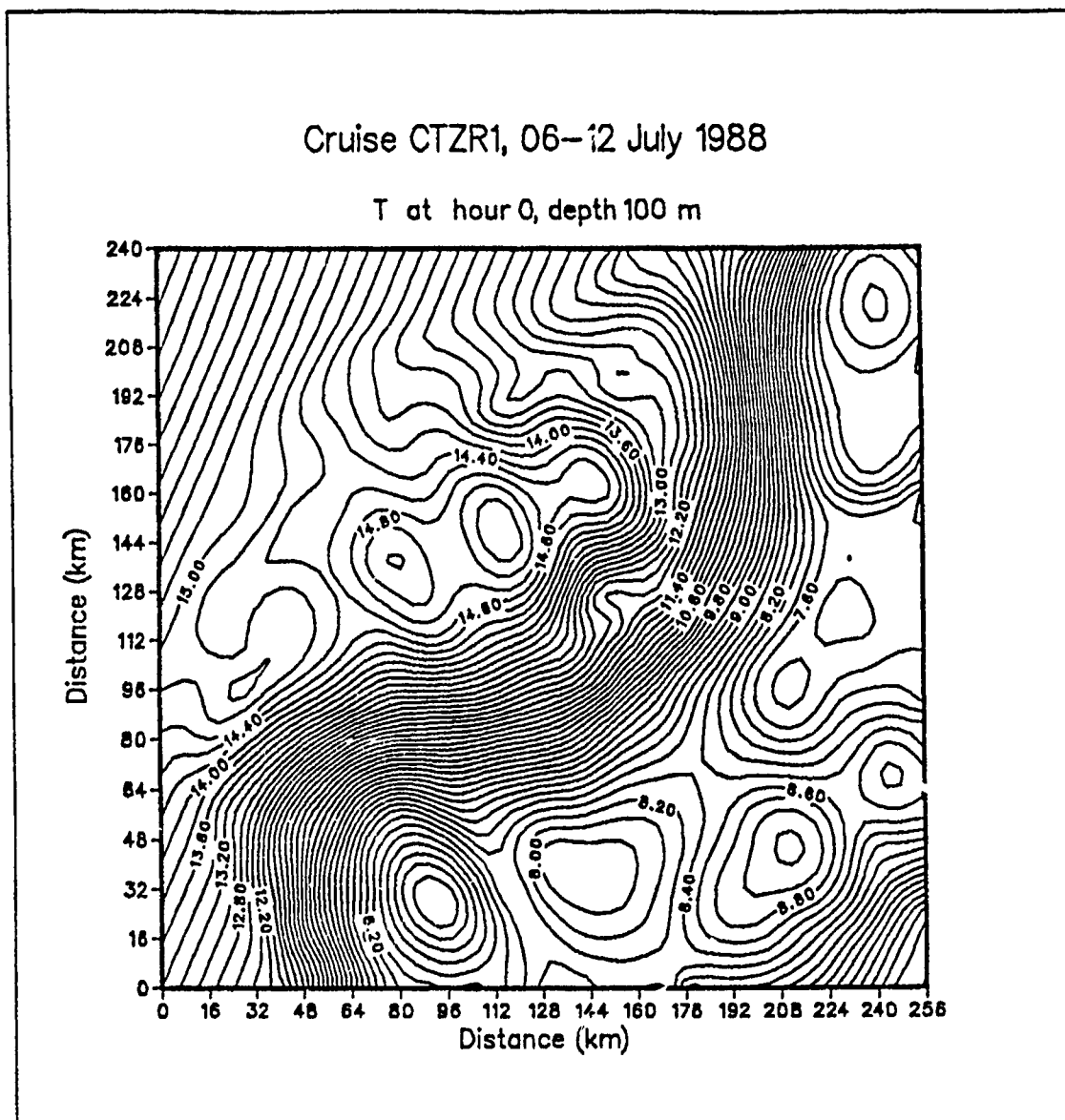
Figure 24.   Apparent Temperature at 100 m Depth, Cruise CTZR1:   Contour interval is 0.2 C.

high velocities observed in the jet. Additionally, the strongest offshore speeds correspond to the area of strongest pressure gradient between the two pressure centers as seen in the 100 m velocity vector field at time 30 hours in Figure 31. The jet is about 50 km wide and can be seen to meander from the northeast to the southwest quadrant of the domain. Jessen and Ramp (1988) reported speeds up to 50 cm sec^{-1} across leg G at the 194 m to 210 m depth as measured by ADCP apparatus.
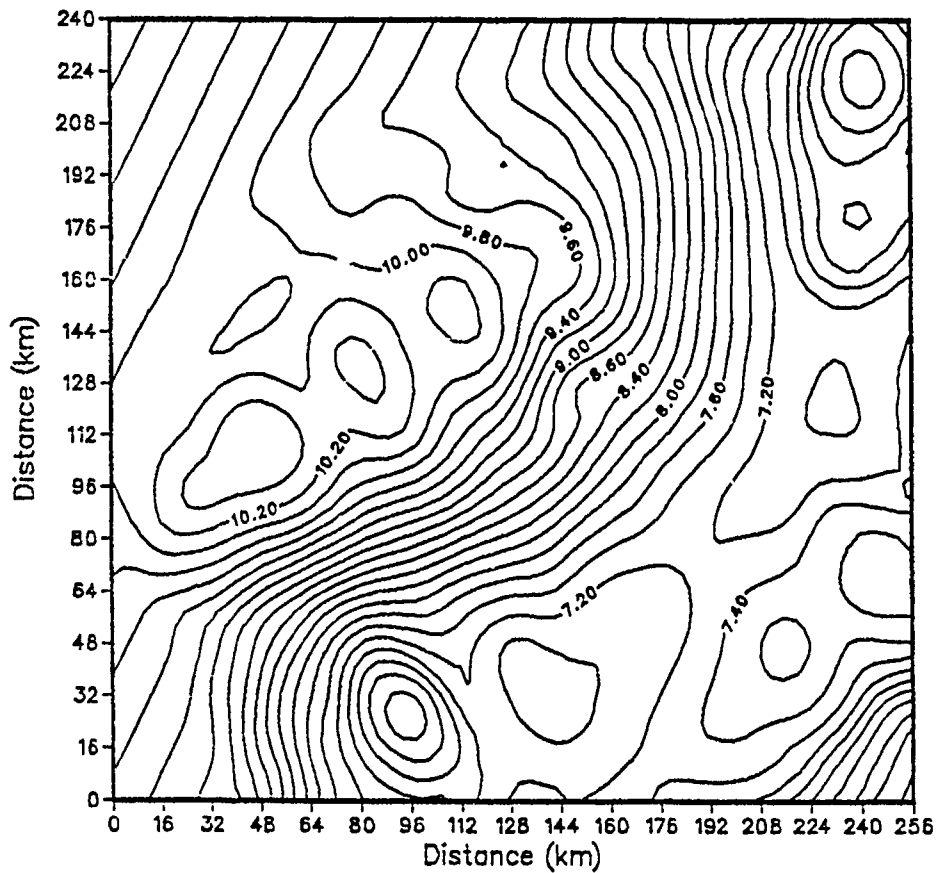
Figure 25. Apparent Temperature at 200 m Depth, Cruise CTZR1: Contour interval is 0.2 C.

The cross-sections of the u-component and v-component velocity fields at time zero are shown in Figure 32 and Figure 33. Both cross-sections run northwest to southeast through the area of greatest pressure gradient (point (32, 96) to (96, 32) in Figure 30). Together the two cross-sections show the large-scale current patterns from the surface to the bottom of the ocean. In the u-component cross-section, offshore surface current speeds are greater than 55 cm sec^{-1}, decreasing to zero near 300 m. Below 300 m,

Figure 26. U Field at Time = 0 h, Depth 100 m, Cruise CTZR1: Dashed lines denote offshore (westward) flow. Solid lines denote onshore (eastward) flow. Contour interval is 2.5 cm sec⁻¹.

onshore flow occurs, with speeds greater than 15 cm sec⁻¹ near 700 m. Flow gradually decreases to zero near 1000 m. The v-component cross-section shows equatorward surface current speeds greater than 45 cm sec⁻¹, decreasing to zero near 300 m. Below 300 m, poleward flow occurs, with speeds greater than 15 cm sec⁻¹ near 600 m. Flow again decreases to zero near 1000 m. The large-scale baroclinic currents associated with the initial temperature fields are significant in the upper 1000 m of the ocean.

Figure 27. V Field at Time = 0 h, Depth 100 m, Cruise CTZR1: Dashed lines denote equatorward flow. Solid lines denote poleward flow. Contour interval is 5.0 cm sec^{-1}.

B. VELOCITY COMPARISON WITH ADCP DATA

A qualitative comparison between CTZR1 model output velocity and ADCP acquired velocity is now given. ADCP velocities from cruise CTZR1 are shown in Figure 34. The solid dots at regular intervals indicate the stations occupied during the cruise. Comparison with the model output velocity vector field at time 30 hours,
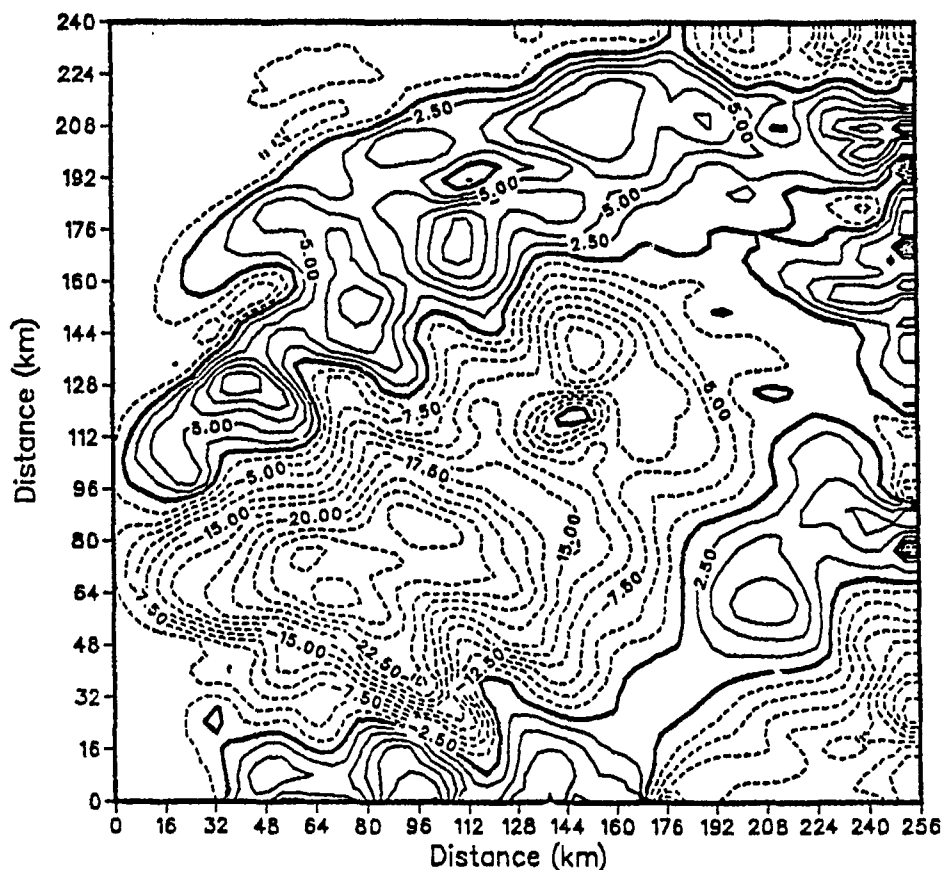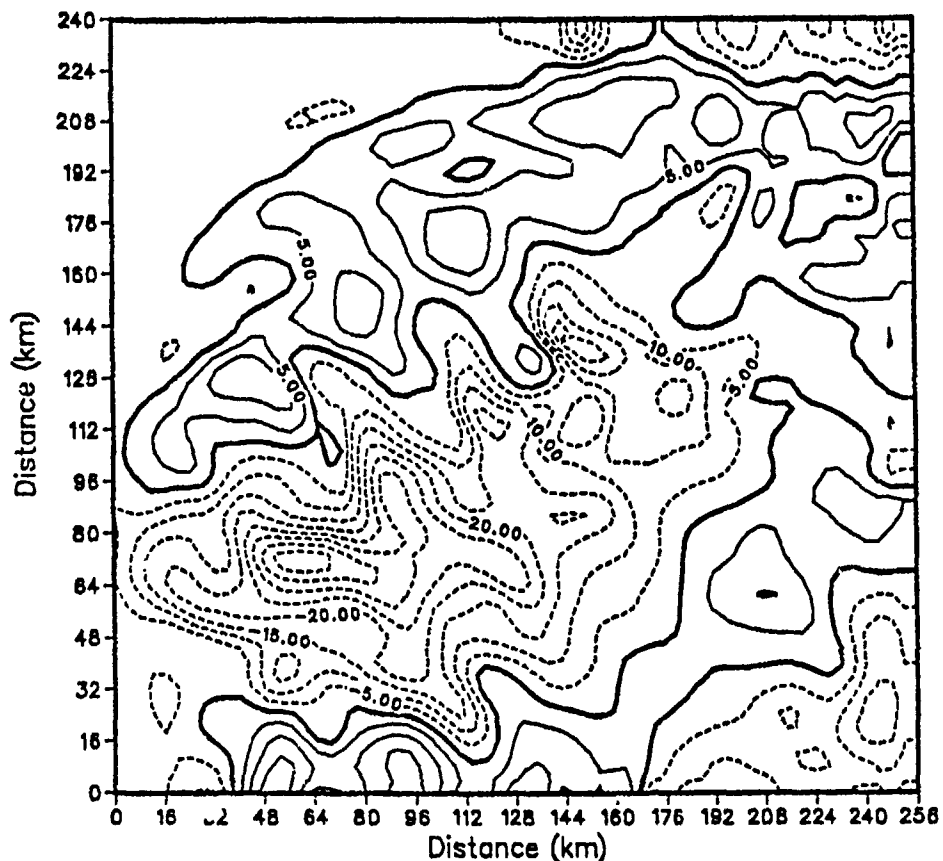
Figure 28. U Field at Time = 30 h, Depth 100 m, Cruise CTZR1:   Dashed lines denote offshore (westward) flow. Solid lines denote onshore (eastward) flow. Contour interval is 5 cm sec^{-1}.

Figure 31, shows good agreement with the position of the jet and the magnitude of the velocities between grid legs F and G.

Model domain cross-section locations (solid lines) are shown in Figure 35. A typical cross-section is shown along grid leg C, Figure 36. The corresponding ADCP cross-section is shown in Figure 37. In the ADCP cross-sections, northwest is to the left and equatorward flows are denoted by solid lines. In the model output cross-sections,

Cruise CTZR1, 06–12 July 1988
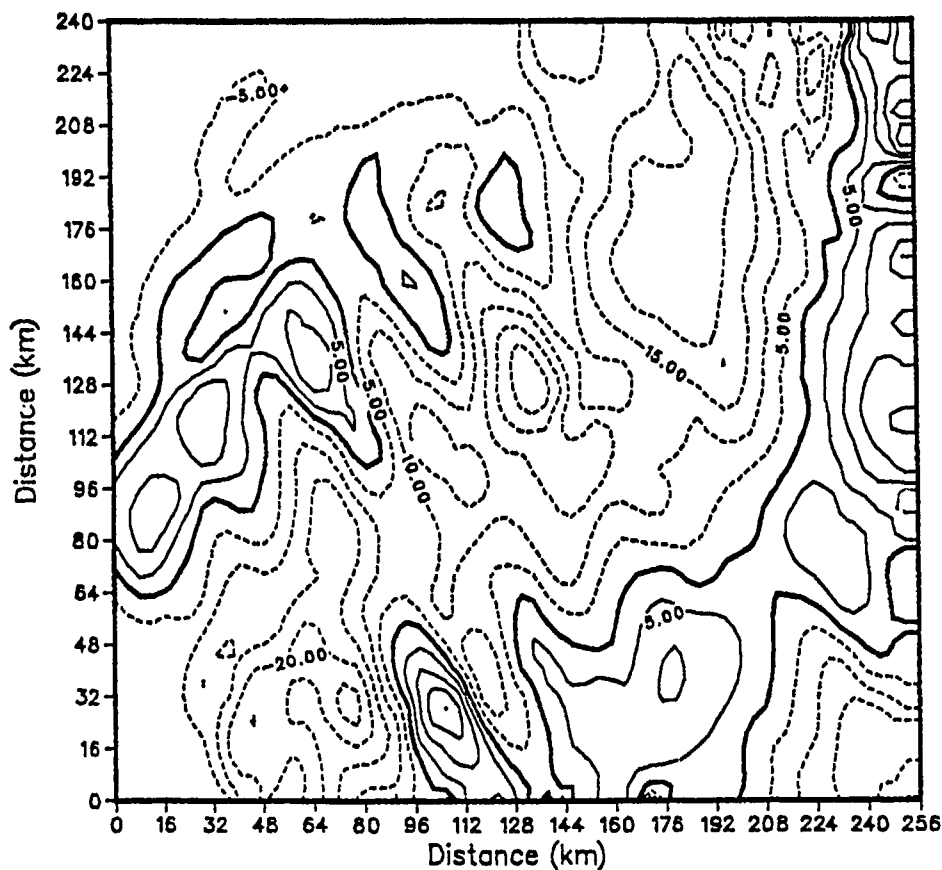
V at hour 30, depth 100 m
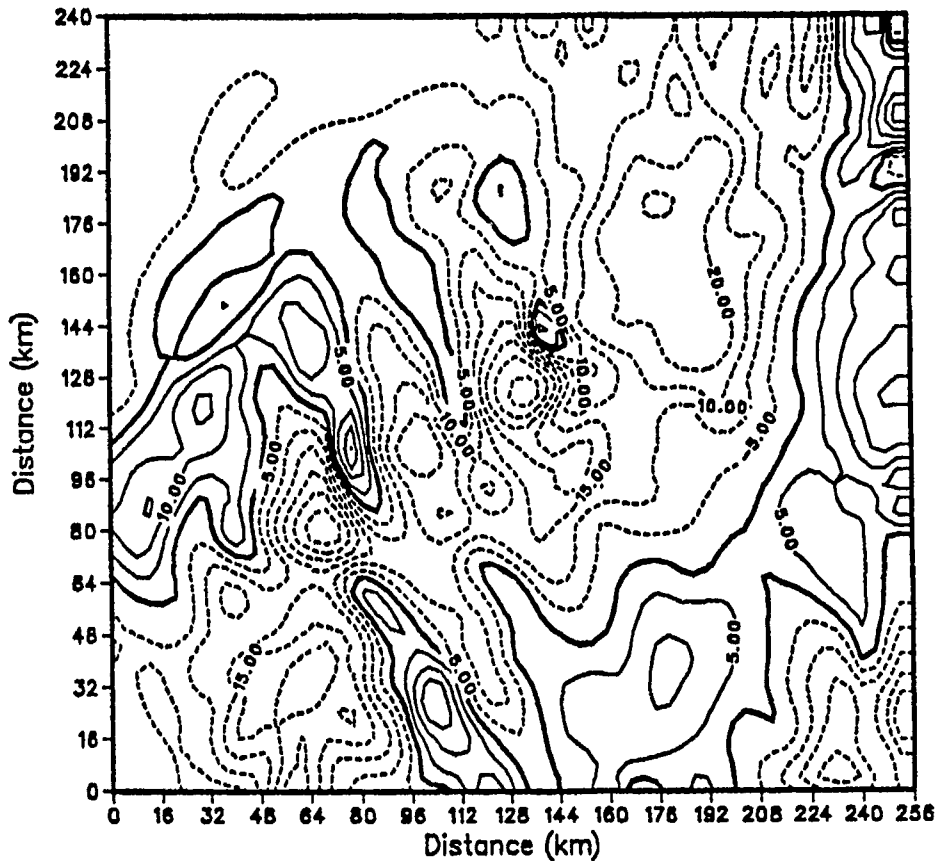
Figure 29. V Field at Time = 30 h, Depth 100 m, Cruise CTZR1: Dashed lines denote equatorward flow. Solid lines denote poleward flow. Contour interval is 5 cm sec^{-1}.

northwest is to the left and equatorward flows are denoted by dashed lines. The core of the jet is readily discernable in both cross-sections, with the model output showing a 60 cm sec^{-1} contour. The model output cross-section shows poleward flow (solid lines) in the southern portion of the cross-section, but the ADCP cross-section shows only equatorward flow in the section for comparison. The ADCP cross-section shows deeper flows below 300 m (the irregular shaded area is the limit of good data, not the bottom

38

Cruise CTZR1, 06–12 July 1988

P at hour 0, depth 100 m
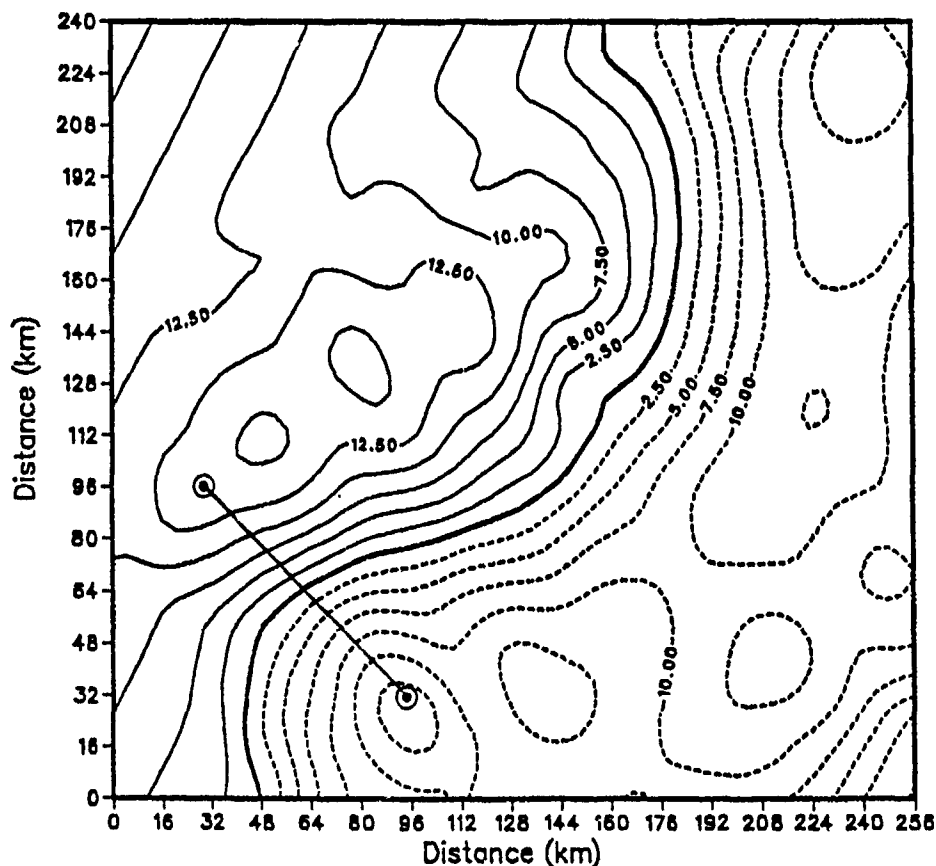
Figure 30. Pressure Field at Time = 0 h, Depth 100 m, Cruise CTZR1: Contour interval is 2.5 cm. The line segment joining points (32, 96) and (96, 32) is the cross-section shown in Figure 32 and Figure 33.

of the ocean), which indicates less shearing flow at 300 m than the model output cross-section, which indicates a level of no motion at 300 m. The model output cross-section shows a broader baroclinic flow with a level of no motion near 300 m. In all the cross-sections (except leg G), the typical difference in surface velocity between the ADCP and model output velocity is 5 cm sec⁻¹ to 10 cm sec⁻¹, with the ADCP velocity usually greater than the model output velocity.
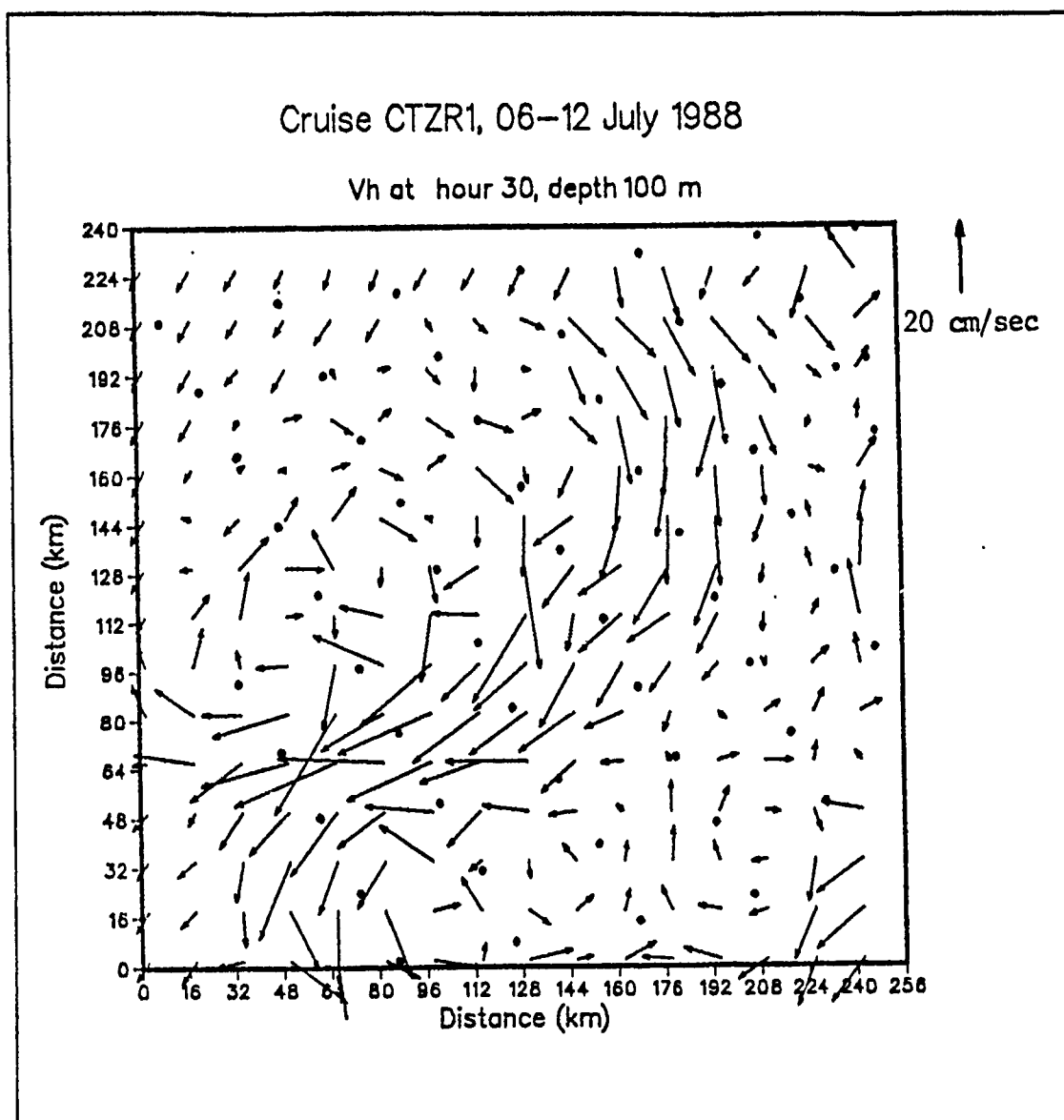
Figure 31. Velocity Vector Field at Time = 30 h, Depth 100 m, Cruise CTZR1: Vectors are plotted at every other point in the model domain. Dots indicate positions of the individual stations of the CTZ grid. Note the strongest flow between grid legs F and G.

The cross-sections across leg G are of note because of the stronger surface flows shown in the ADCP velocity cross-section, Figure 38, which is about 30 cm sec^{-1} higher than the model output cross-section, shown in Figure 39. The ADCP velocity cross section shows surface speeds greater than 80 cm sec^{-1}. Jessen and Ramp (1988) reported
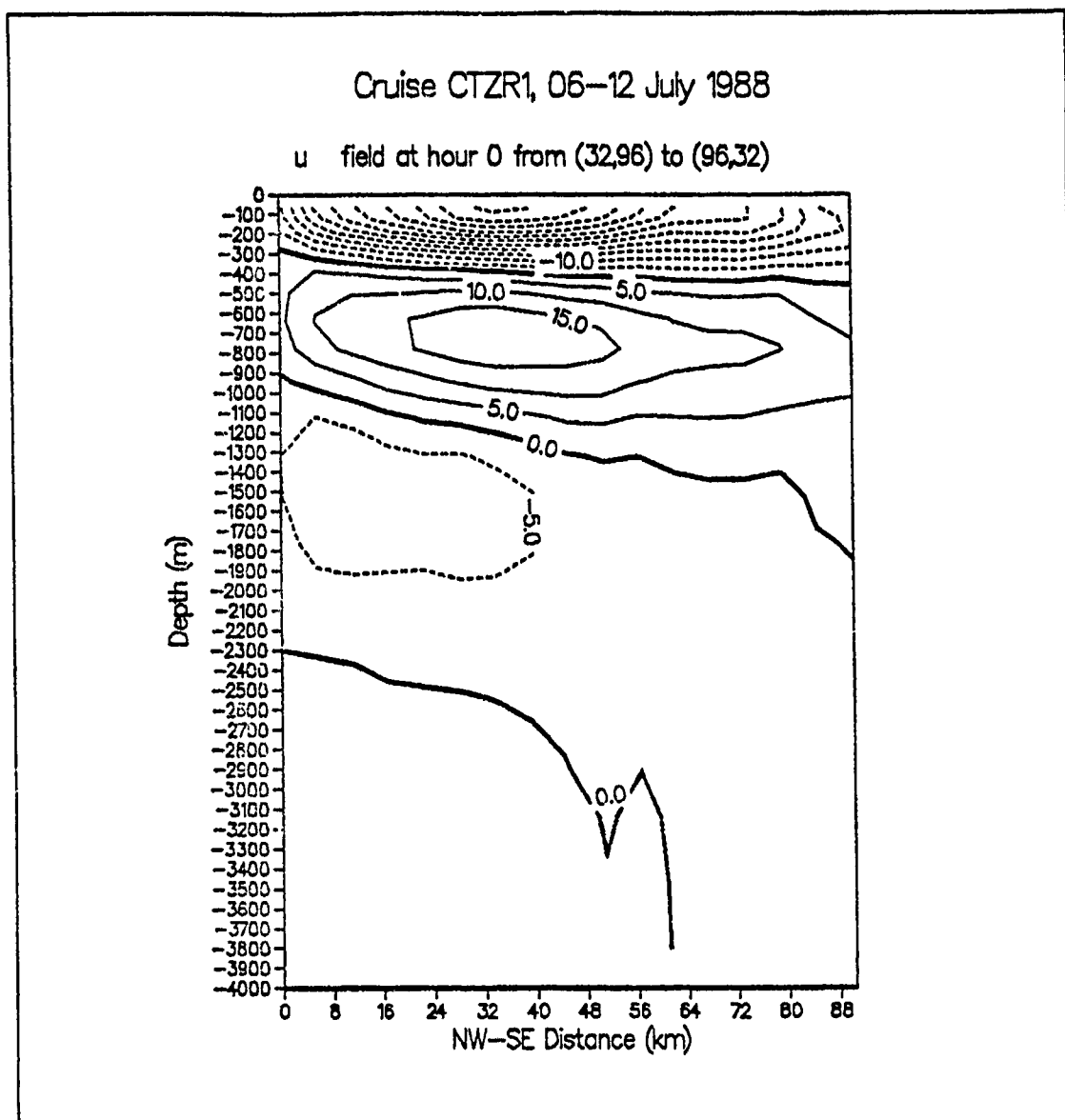
Figure 32. U Field Cross-section, Time = 0 h, Depth 100 m, Cruise CTZR1: Northwest is to the left. Westward flow is denoted by dashed lines. Eastward flow is denoted by solid lines. Contour interval is 2.5 cm sec⁻¹. Location of the cross-section is shown in Figure 30.

surface speeds up to 100 cm sec⁻¹. The model output cross-section only shows surface speeds greater than 55 cm sec⁻¹.

It must be remembered that the effect of the objective analysis interpolation between 20 nm separated stations inevitably underestimates geostrophic flow with small horizontal scales; that is, tight gradients in the actual flow field will be smoothed out, re-

Cruise CTZR1, 06–12 July 1988

v field at hour 0 from (32,96) to (96,32)
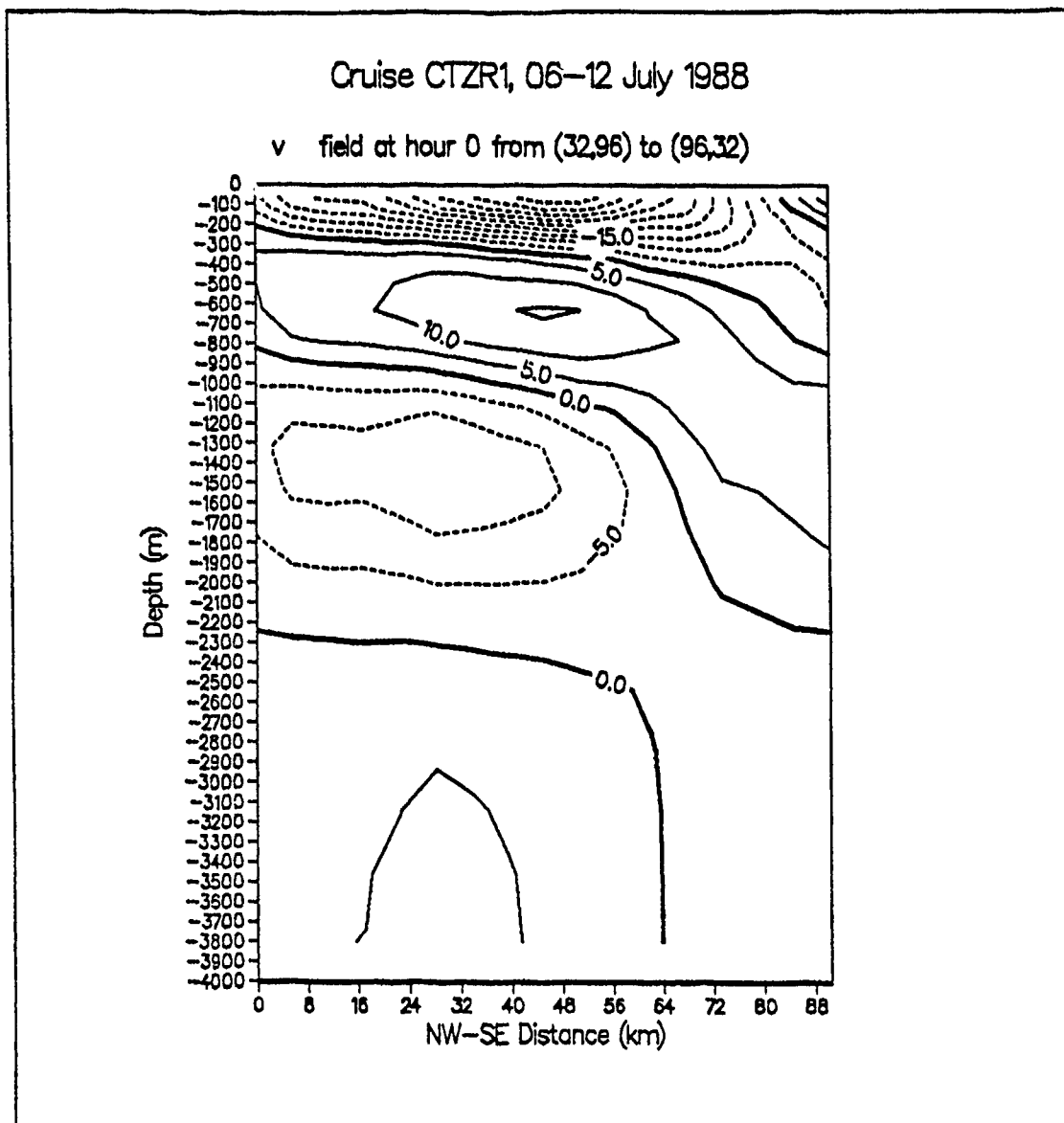
Figure 33. V Field Cross-section, Time = 0 h, Depth 100 m, Cruise CTZR1: Northwest is to the left. Equatorward flow is denoted by dashed lines. Poleward flow is denoted by solid lines. Contour interval is 5.0 cm sec⁻¹. Location of the cross-section is shown in Figure 30.

sulting in lower analyzed speeds and less horizontal resolution in the plotted objectively analyzed flow field. This unavoidable result of the objective analysis is a compromise between the cost and resources available to acquire quasi-synoptic data within a reasonable amount of time and the need to sample the flow field adequately to fully define the actual flow. Additionally, the currents measured by the ADCP will have
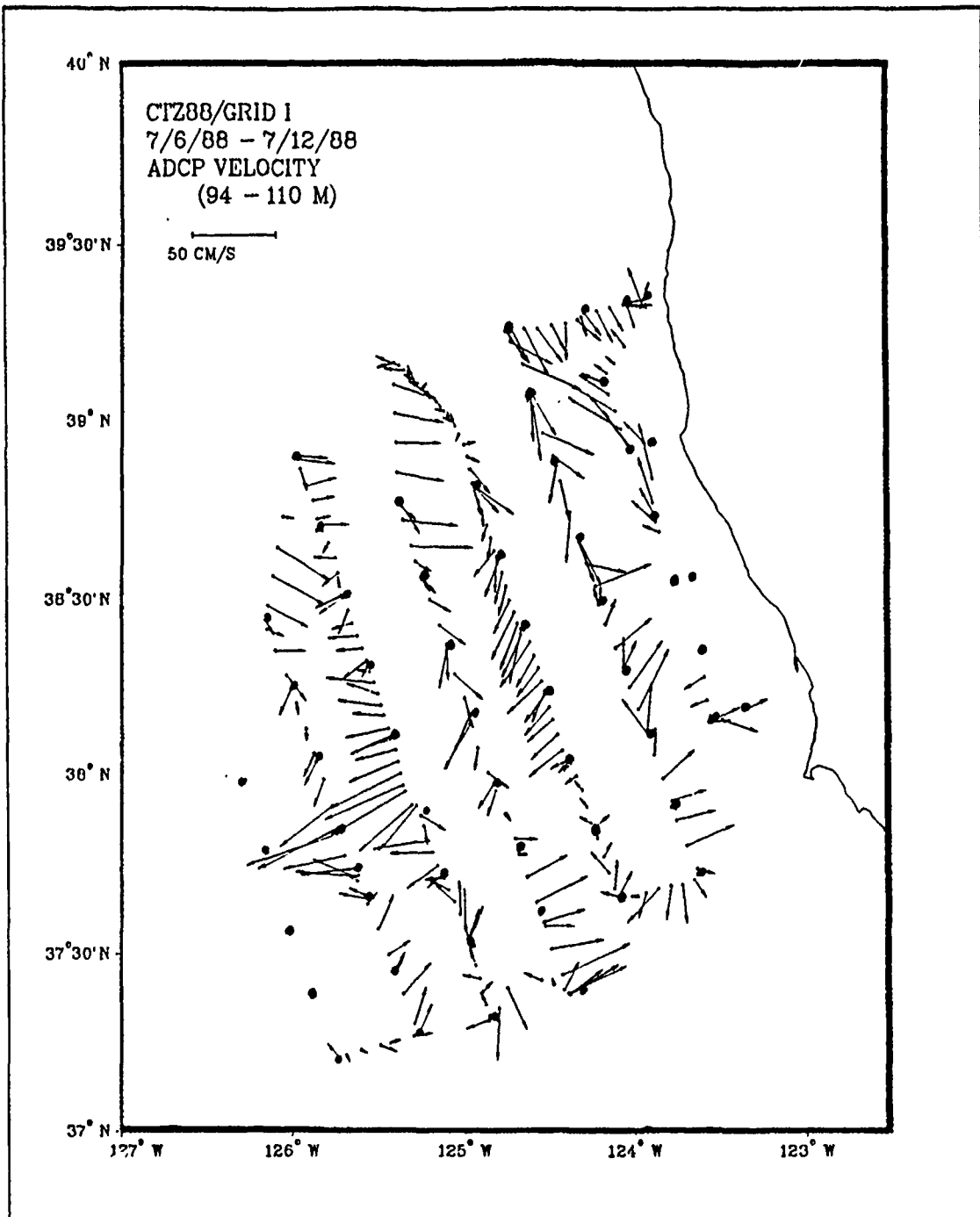
Figure 34. ADCP Velocity (94-110 m) for Cruise CTZR1: Regularly spaced do†s are stations occupied during the cruise. Note strongest flows between grid legs F and G.
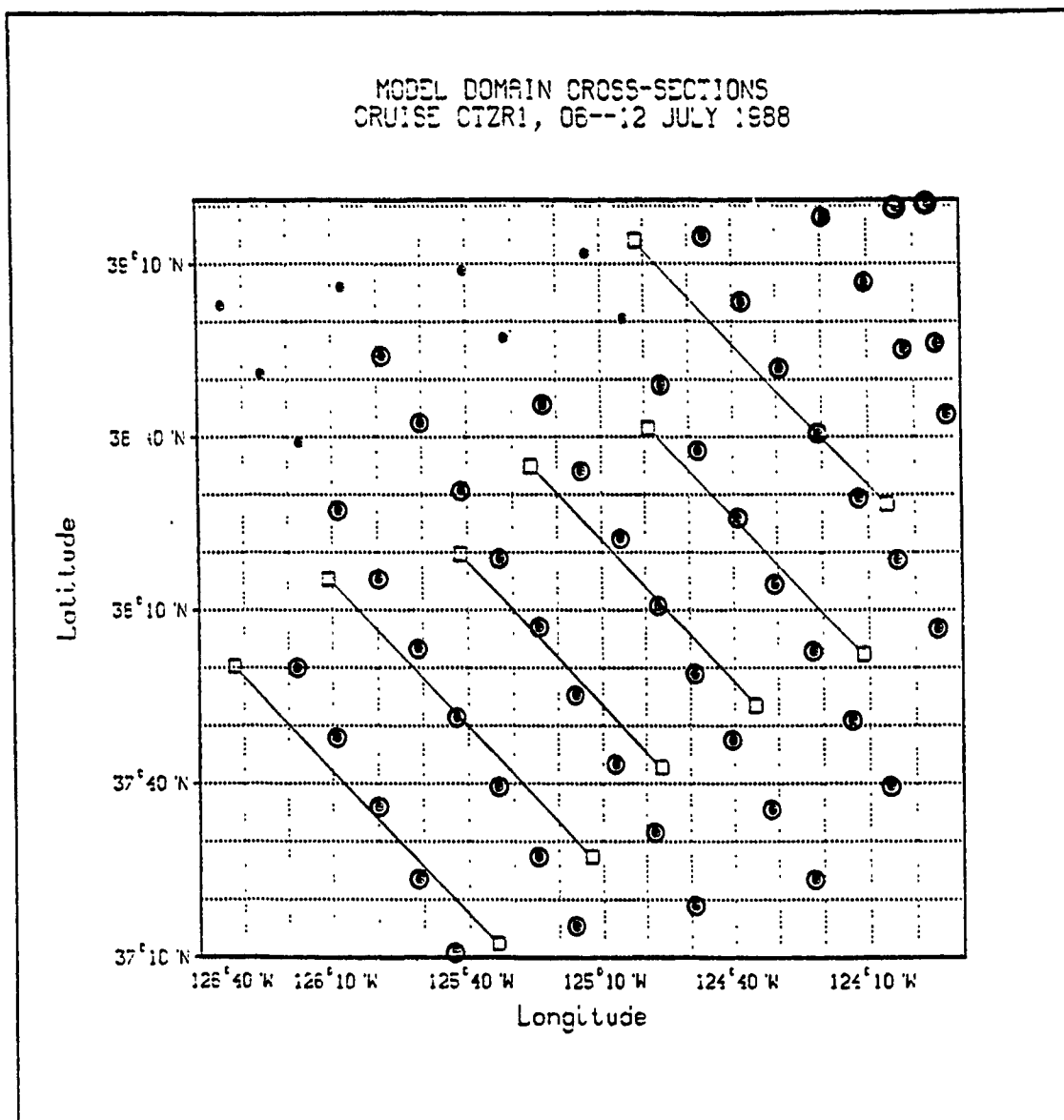
Figure 35. Model Domain Cross-sections, Cruise CTZR1: Circled dots are stations occupied during the cruise. Solid lines show location of model cross-sections. Model cross-sections of legs C and G will be shown for comparison with ADCP data.

ageostrophic components associated with them; e. g., internal waves, tides, inertial oscillations, and Ekman transport.

All in all, the model output cross-sections show a less complicated flow field and a shallower level of no motion than the ADCP velocity cross-sections. To achieve a more detailed and realistic deep flow, the barotropic mode should be incorporated into the
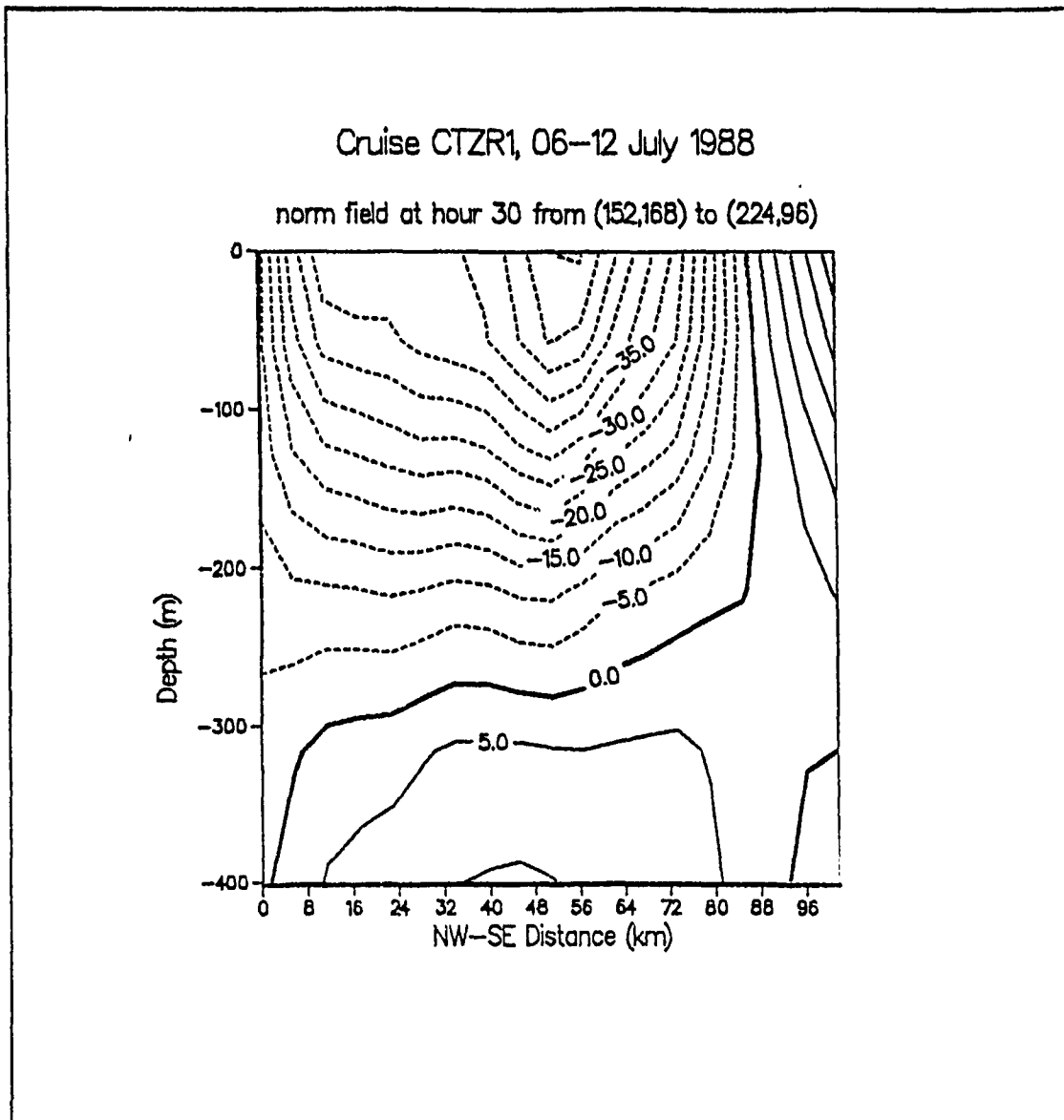
Figure 36. Model Velocity Cross-section for Grid Leg C, Cruise CTZR1: Dashed lines indicate equatorward flow. Solid lines indicate poleward flow. Northwest is to the left. Contour interval is 5 cm sec^{-1}.

model. A complete statistical verification of the ADCP acquired velocity with model output velocity is considered to be another study.

C. VERTICAL VELOCITY

Vertical velocity for CTZR1 at 30 hours is shown in Figure 40. The solid lines denote upwelling areas and the dashed lines denote downwelling areas. Strong mesoscale

45
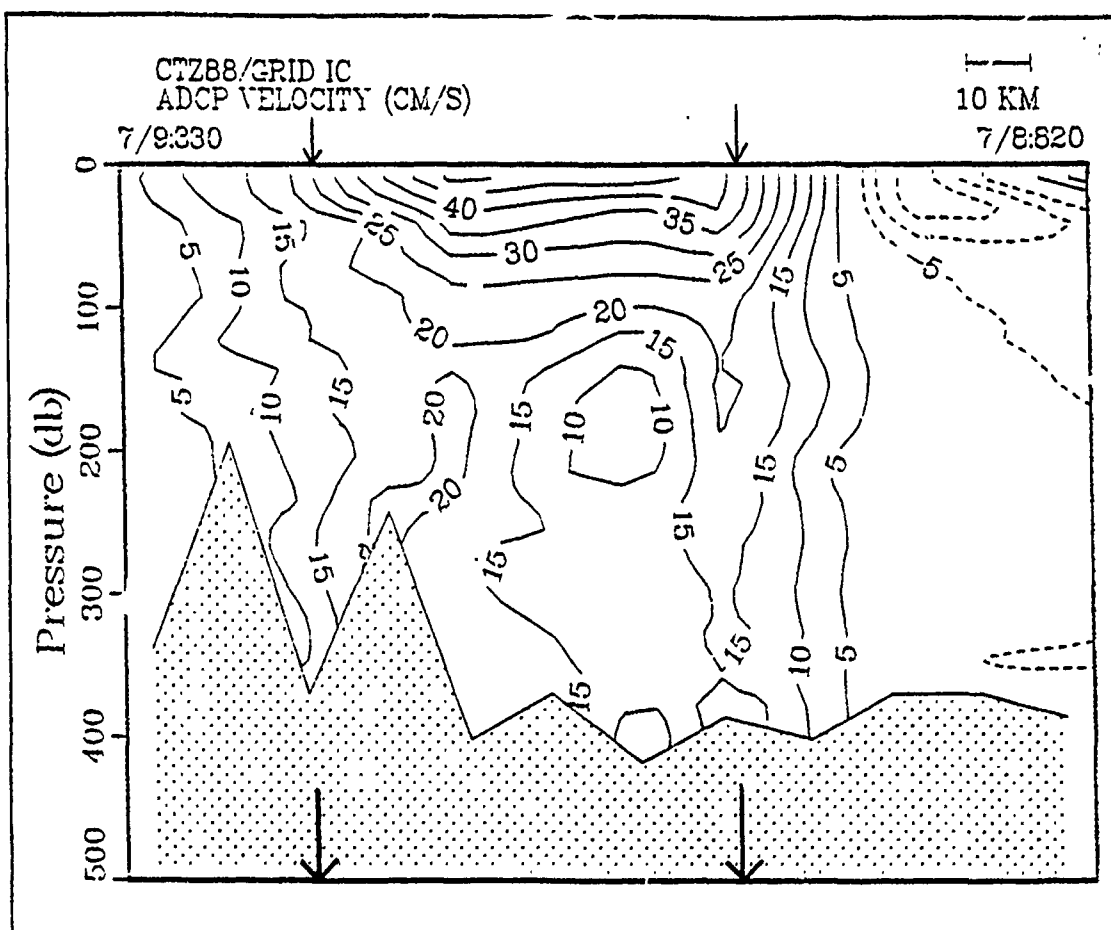
Figure 37.   ADCP Velocity Cross-section Along Leg C for Cruise CTZR1:   Ar-
rows indicate boundaries of corresponding model output cross-section
for comparison.   Solid lines indicate equatorward flow.   Dashed lines
indicate poleward flow   Northwest is to the left.   Contour interval is 5
cm sec⁻¹.

patterns are clearly evident. The model calculated vertical velocity by a finite difference
integration of the continuity equation as given in integral form by

$$ - \int_{-H}^{z} (\frac{\partial u}{\partial x} + \frac{\partial v}{\partial y}) \, dz \; = \; \int_{-H}^{z} \frac{\partial w}{\partial z} \, dz \; = \; w(z) $$

The model vertical velocity value was scaled by a factor of 100 for plotting purposes,
so the contour values on the vertical velocity figures must be divided by 100 to obtain
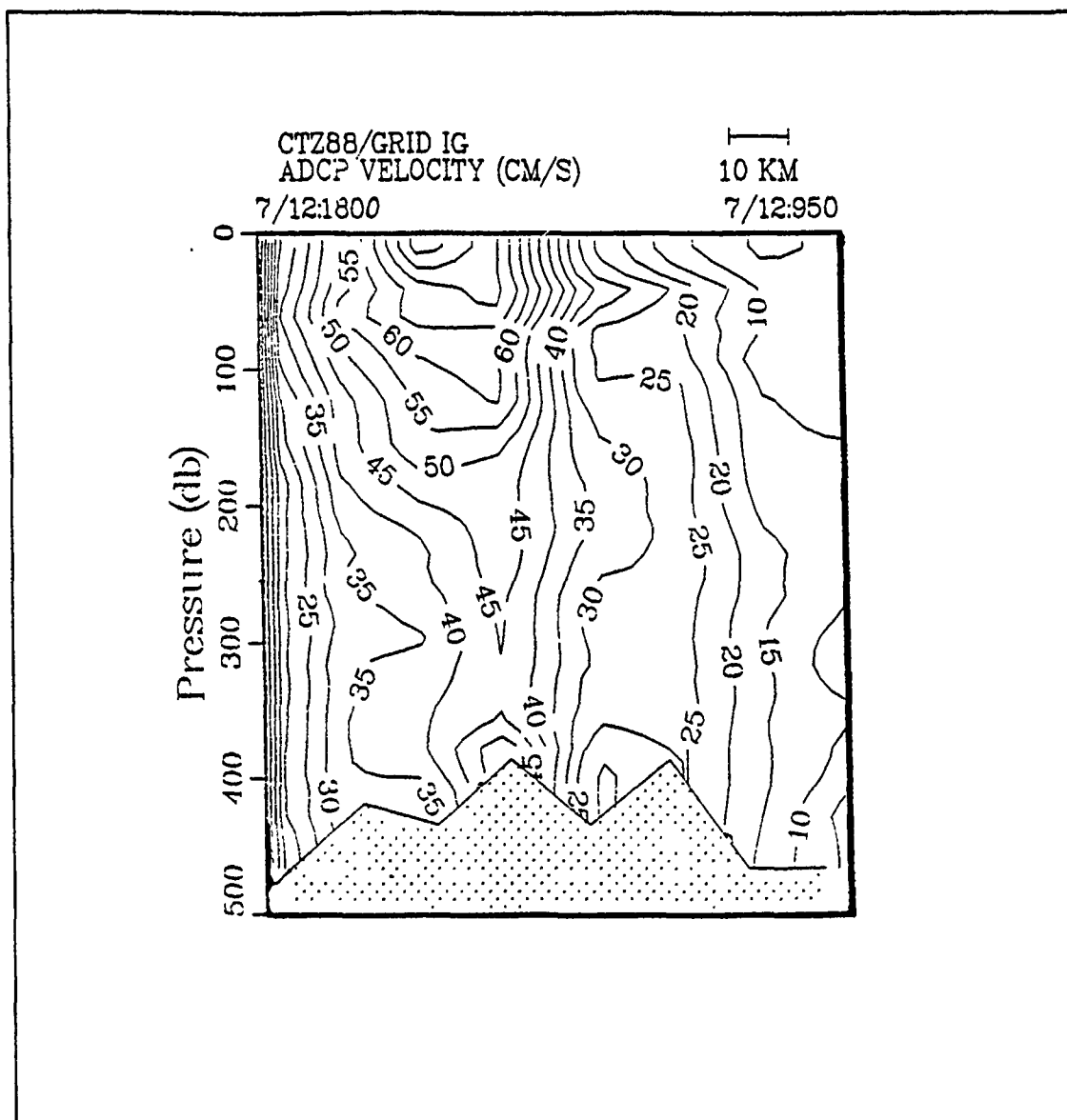
Figure 38. ADCP Velocity Cross-section Along Leg G for Cruise CTZR1: Solid lines indicate equatorward flow. Northwest is to the left. Contour interval is 5 cm sec⁻¹.

the values calculated by the model. The maximum upwelling speed was greater than .30 cm sec⁻¹ or 260 m day⁻¹. The maximum downwelling speed was greater than .60 cm sec⁻¹ or 520 m day⁻¹. Washburn *et al.*, (1990), reported downwelling rates of 6 to 10 m day⁻¹ during leg 2 (6 to 18 July 1988) of the R/V THOMAS WASHINGTON cruise, which was coincident with the cruise dates for cruises CTZR1 and CTZR2.

47
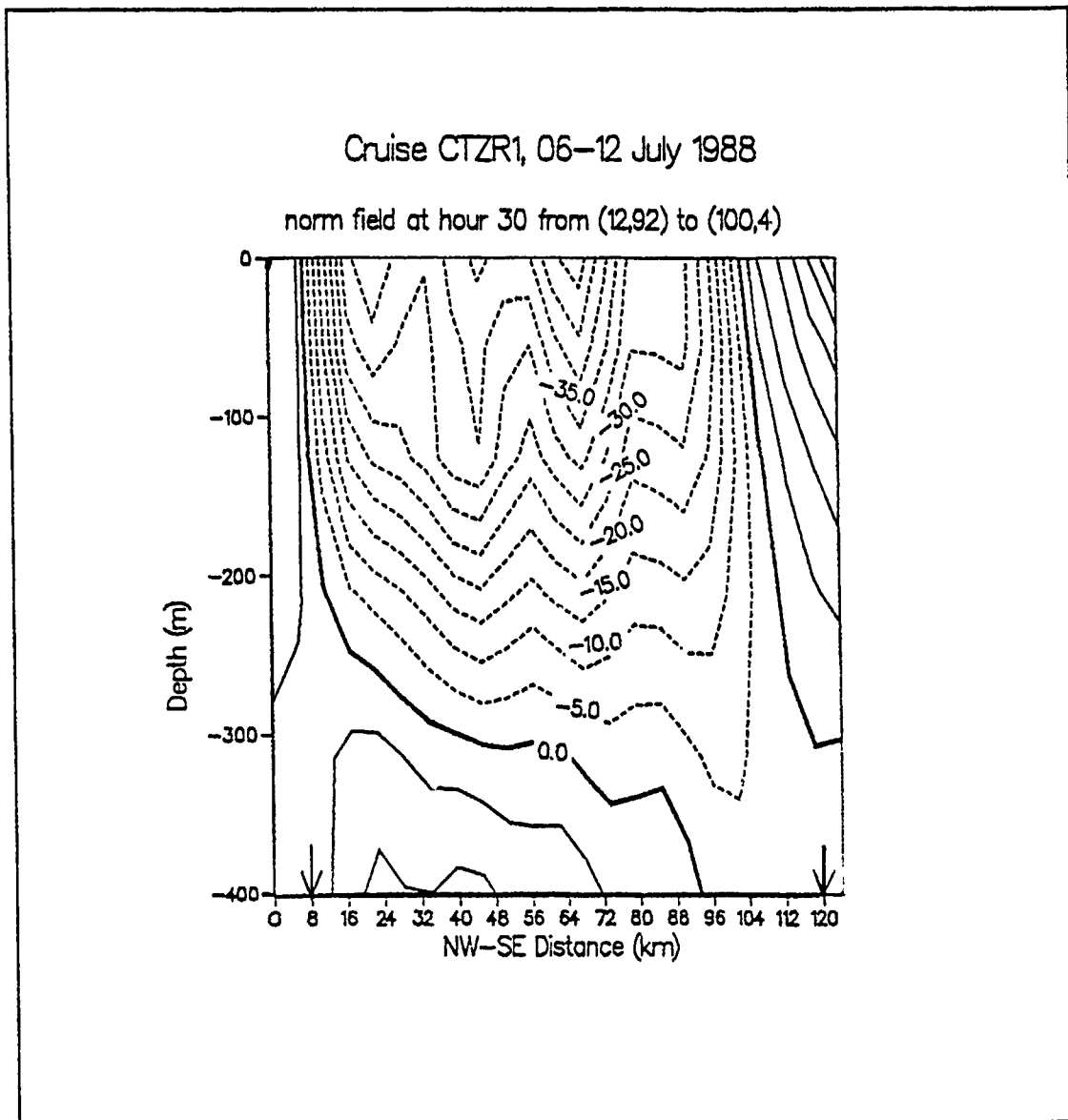
Figure 39. Model Velocity Cross-sections for Leg G, Cruise CTZR1: Arrows indicate boundaries of corresponding ADCP velocity cross-section for comparison. Equatorward flow is denoted by dashed lines. Poleward flow is denoted by solid lines. Northwest is to the left. Contour interval is 5 cm sec^{-1}.

The areas of downwelling and upwelling are associated with the small scale patterns of pressure (Figure 30). This can be observed by carefully noting the positions of the areas of downwelling and upwelling and comparing them to the areas of troughing and ridging in the pressure pattern. The areas of convergence are associated with troughs,

Figure 40. Model Vertical Velocity Field at Time 30 h, Depth 100m, Cruise CTZR1: Downwelling is denoted by dashed lines. Upwelling is denoted by solid lines. Contour interval is .10 cm sec^{-1}.

and areas of divergence are associated with ridges. A discussion of this relationship will be pursued in the next chapter.

Washburn *et al.*, (1990) identified downwelling areas using bio-optical data. The points he identifies as areas of downwelling are shown in Figure 41 and Figure 42.

The major results of this study are contained in the following three figures. The first figure, Figure 43, is of the CTZR1 model vertical velocity field at 30 hours with points
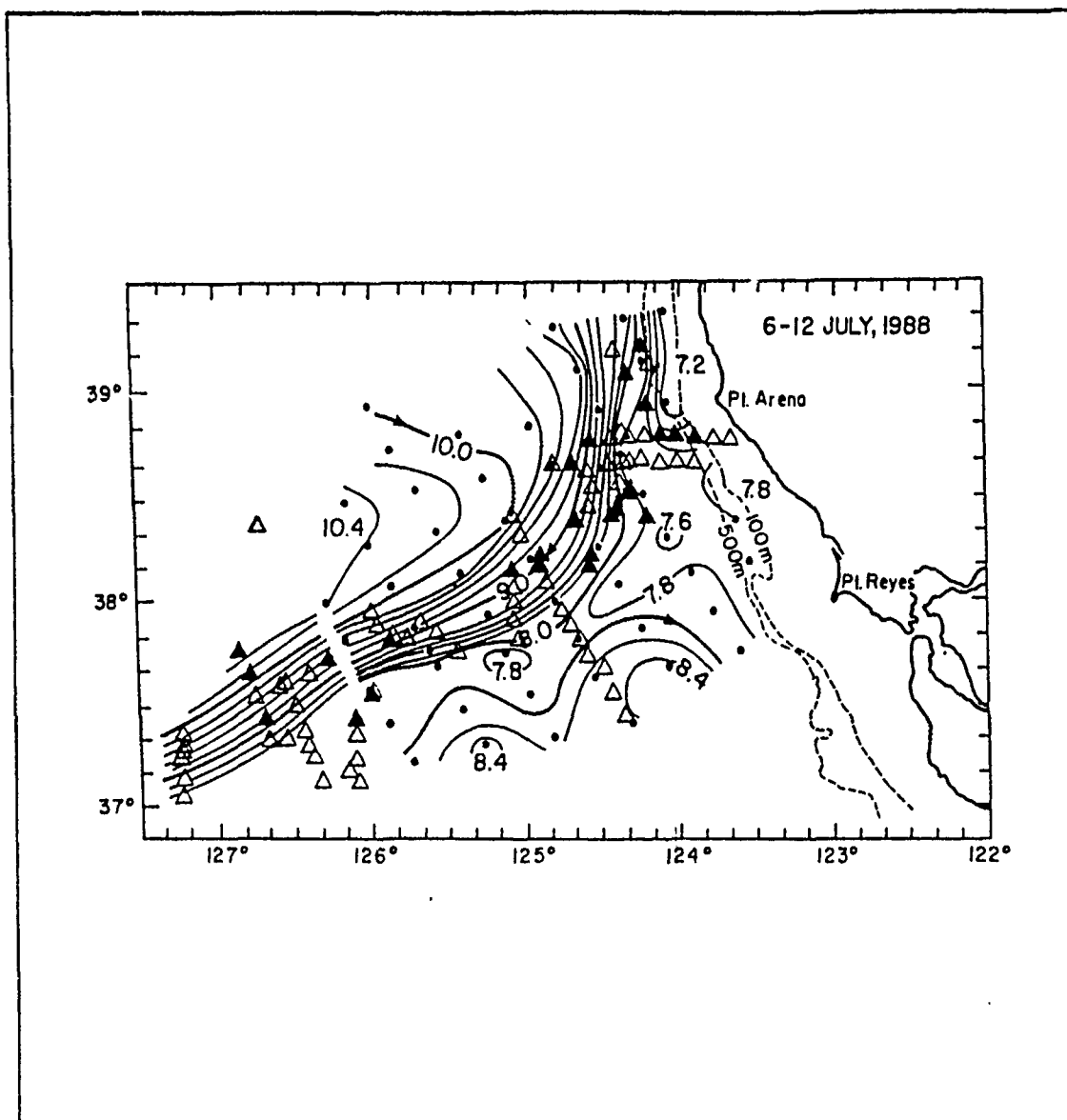
Figure 41.   Locations of All Stations During Leg 2 of R/V THOMAS
WASHINGTON Survey (Triangles): Filled triangles indicate stations
with downwelled water masses. Contours of geopotential anomaly
(0/500 dbar) are from cruise CTZR1 (6-12 July 1988). Offshore exten-
sion of geopotential anomaly contours from R/V THOMAS
WASHINGTON survey (from Washburn *et al.*, 1990).

identified by Washburn *et al.*, (1990) as downwelling areas plotted onto the model ver-
tical velocity field. Of the 33 points plotted, 26 occurred in downwelling areas (dashed
lines) and seven points (filled in) occurred in upwelling areas (solid lines). Thus, an in-
dependent estimate of downwelling in the CTZ has verified the model results, although
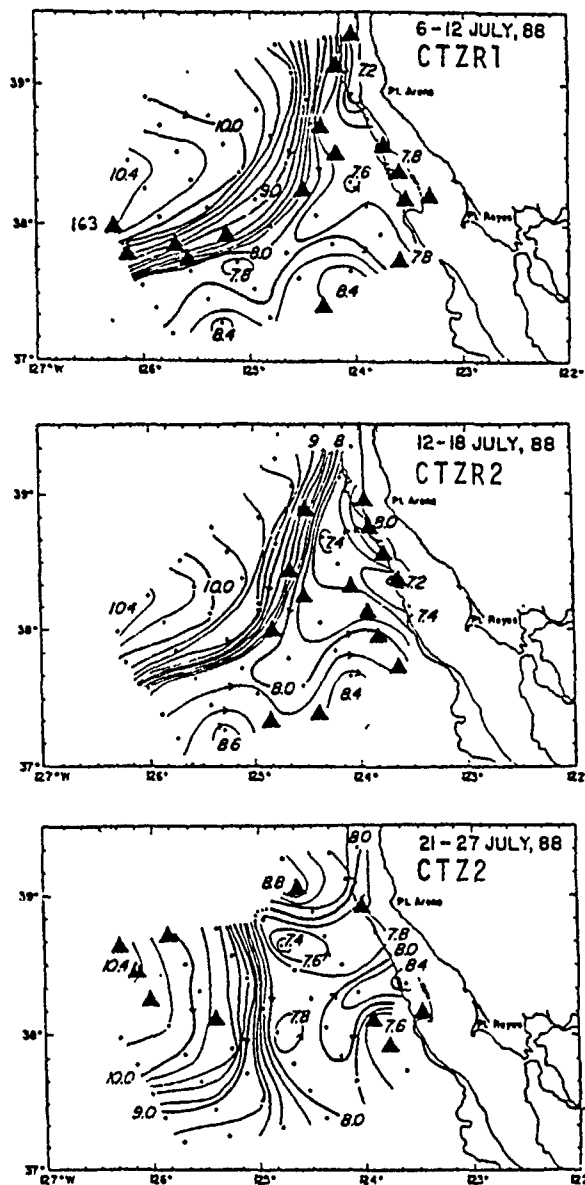
Figure 42.   Locations of Stations Containing Downwelled Water Masses: The top
figure is from cruise CTZR1, the middle figure is from cruise CTZR2,
and the bottom figure is from cruise CTZ2 (from Washburn *et al.*,
1990).

in a somewhat 'spotty' manner. This 'spottiness' in the verification charts for cruises CTZR1, CTZR2, and CTZ2 will be addressed in the next chapter. The points were from the 6 to 12 July 1988 cruises of the R/V THOMAS WASHINGTON and R/V POINT SUR.

The second figure, Figure 44, shows the points identified from cruise CTZR2 as downwelling areas plotted on the model vertical velocity field at time 30 hours. Of the ten points plotted, eight points occurred in downwelling areas, and only two points occurred in upwelling areas.

The third figure, Figure 45, shows the points identified from cruise CTZ2 as downwelling areas plotted on the model vertical velocity field at 30 hours. Of the eight points plotted, four occurred in downwelling areas and four occurred in upwelling areas.

For all three plots, of the 51 points identified as downwelling points, 38 points (75%) occurred in downwelling areas and 13 occurred in upwelling areas.

The magnitude of the mesoscale vertical velocity fields as calculated by the model were on the order of .05 cm sec^{-1} for CTZ2, .10 cm sec^{-1} for CTZR1, and .25 cm sec^{-1} for CTZR2. The unusually high order of magnitude of vertical velocity for cruise CTZR2 is most probably a result of the lack of objectively analyzed data below 250 m for this cruise. Since part of the data processing involved fitting an exponential profile to the last two points of the calculated mean apparent temperature profile, an isothermal condition occurs at relatively shallow depth (1500 m), as seen in Figure 46. The resulting dynamical modes have large amplitudes at depths shallower than 250 m, and the value of the dynamical modes is essentially zero near 1500 m (Figure 47).

The resulting extrapolation of apparent temperature to deep depths using dynamical modes was, therefore, forced by the slope of the relatively short (as compared to 4000 m) 250 m apparent temperature profile. Evidently, 250 m of temperature data are not sufficient for the accurate extrapolation of temperature to depth using dynamical modes.
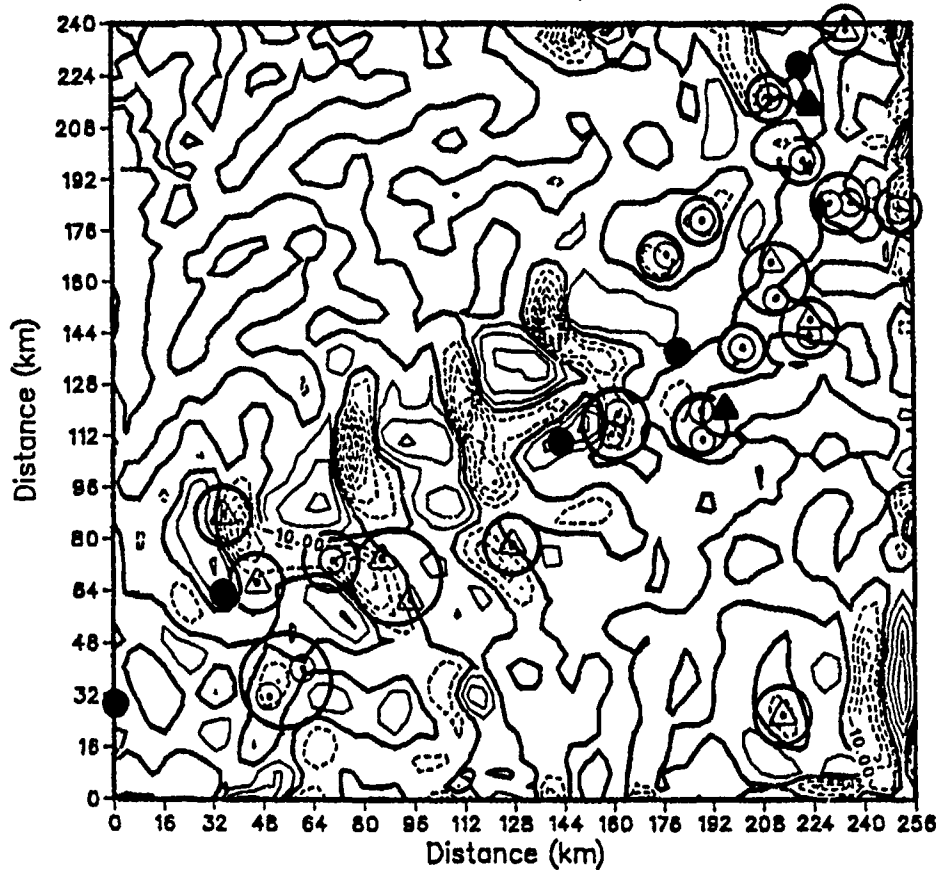
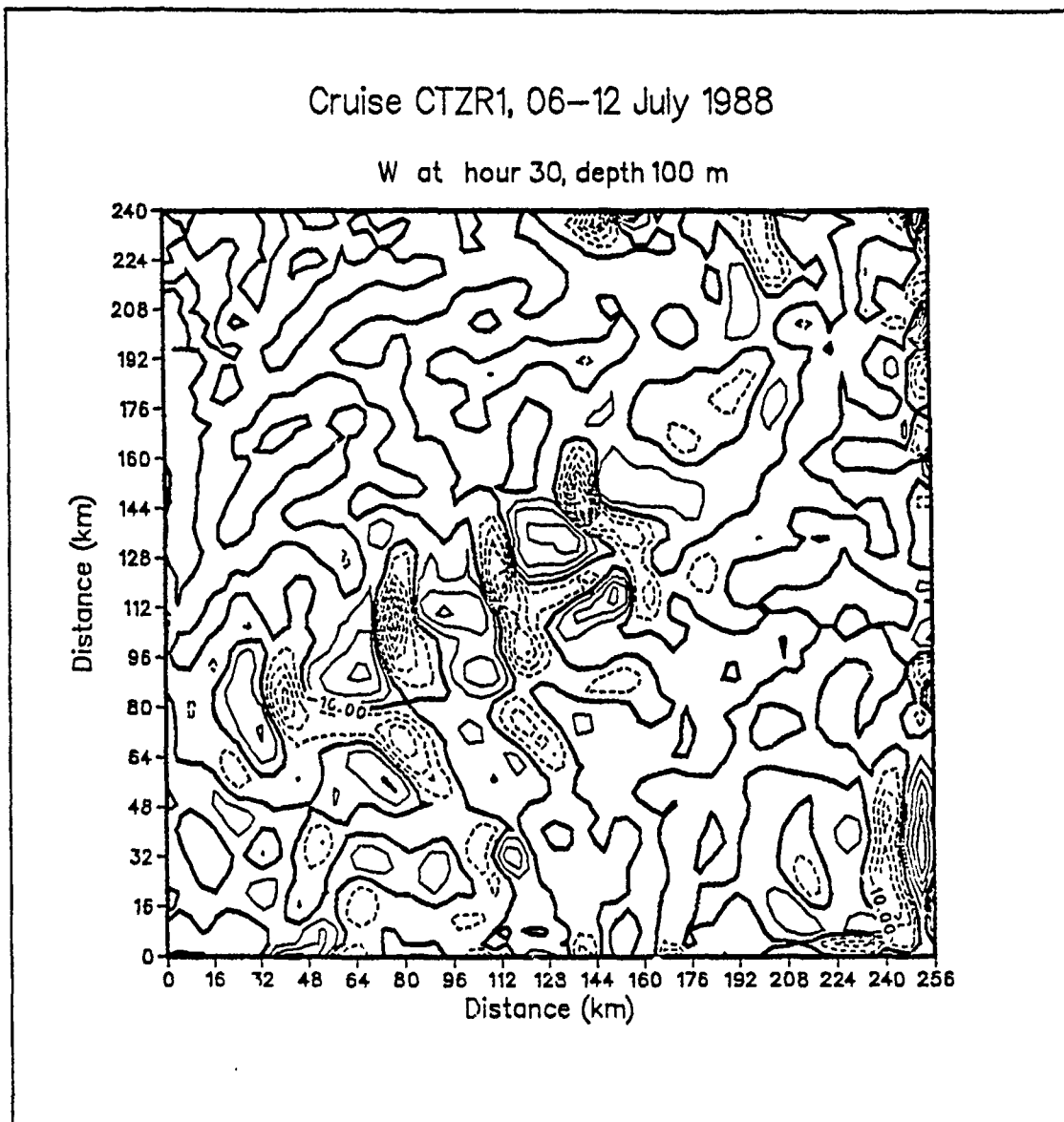Figure 43. Verification of Model Vertical Velocity Field at Time 30 h, Depth 100m, Cruise CTZR1: Downwelling is denoted by dashed lines. Upwelling is denoted by solid lines. Contour interval is 0.1 cm sec^{-1}. The points identified as downwelling areas by Washburn *et al.*, (1990) and occurring in model simulated downwelling areas are circled with a heavy line. Points identified as downwelling areas but occurring in model simulated upwelling areas are shaded.

53

Cruise CTZR2, 13–18 July 1988

W at hour 30, depth 100 m
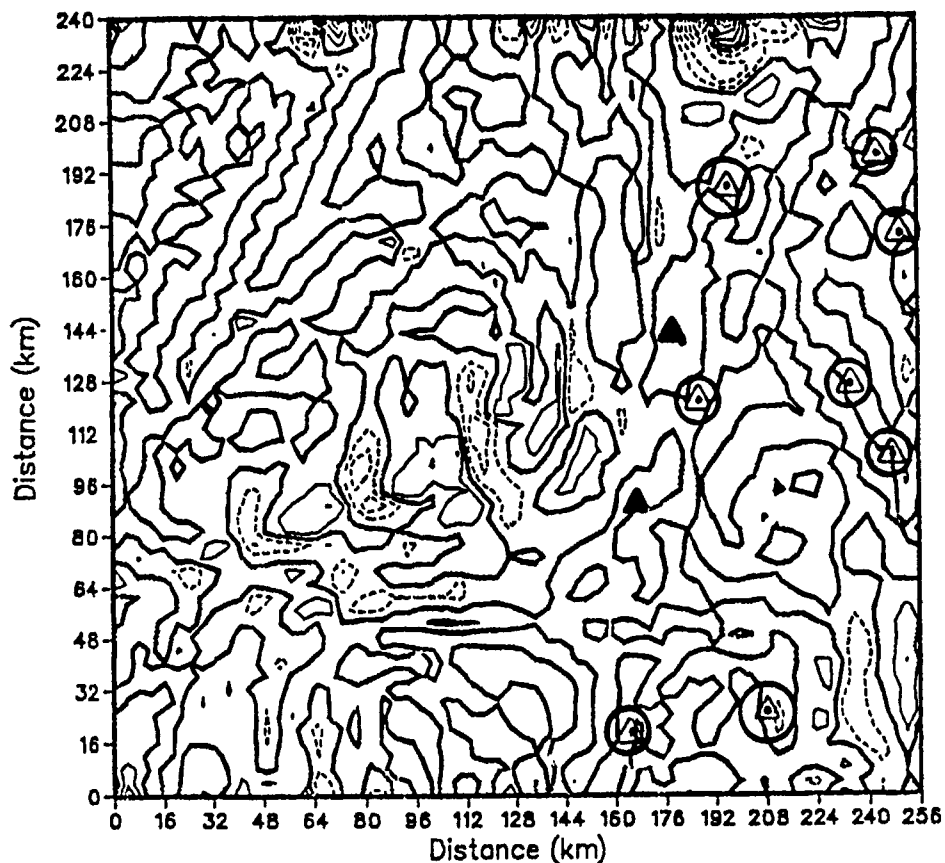
Figure 44. Verification of Model Vertical Velocity Field at Time 30 h, Depth 100m, Cruise CTZR2: Downwelling is denoted by dashed lines. Upwelling is denoted by solid lines. Contour interval is 0.25 cm sec^{-1}. The points identified as downwelling areas by Washburn *et al.*, (1990) and occurring in model simulated downwelling areas are circled with a heavy line. Points identified as downwelling areas but occurring in model simulated upwelling areas are shaded.

Cruise CTZ2, 22–26 July 1988

W at hour 30, depth 100 m
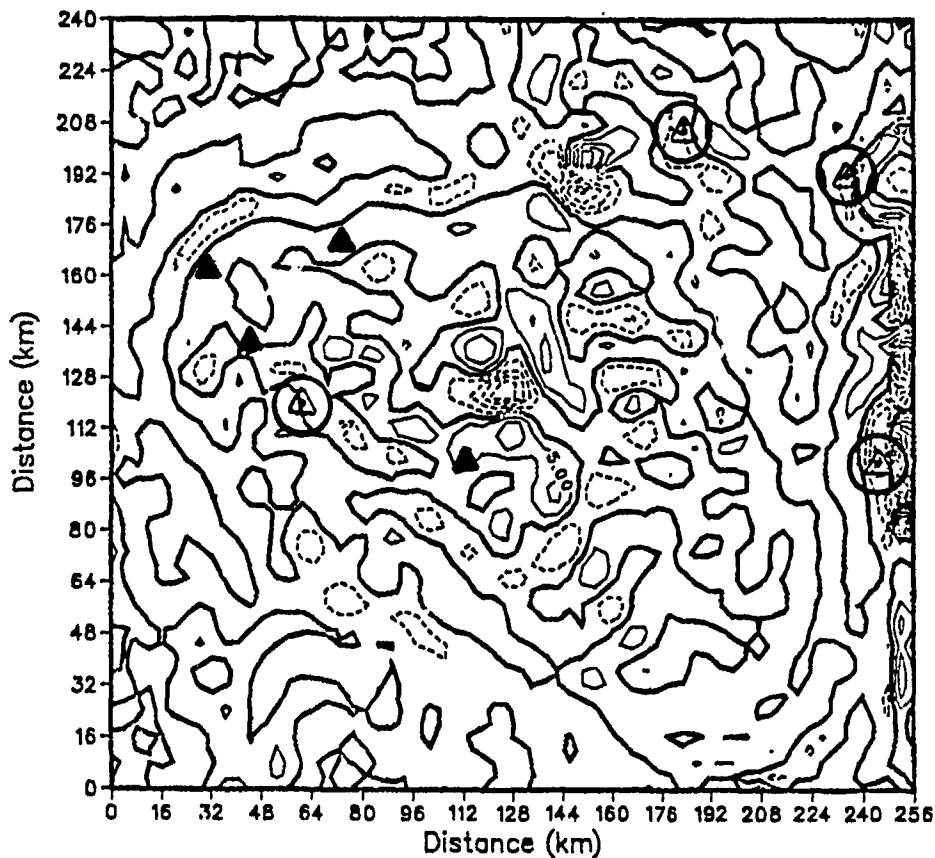
Figure 45. Verification of Model Vertical Velocity Field at Time 30 h, Depth 100m, Cruise CTZ2: Downwelling is denoted by dashed lines. Upwelling is denoted by solid lines. Contour interval is 0.05 cm sec^{-1}. The points identified as downwelling areas by Washburn *et al.*, (1990) and occurring in model simulated downwelling areas are circled with a heavy line. Points identified as downwelling areas but occurring in model simulated upwelling areas are shaded.

MEAN APPARENT TEMPERATURE (C)
VERSUS DEPTH (M)
CRUISE CTZR2
13-18 JULY 1988

Figure 46.   Plot of Mean Apparent Temperature Versus Depth, Cruise
CTZR2:   Note the isothermal condition beginning near 1500m.
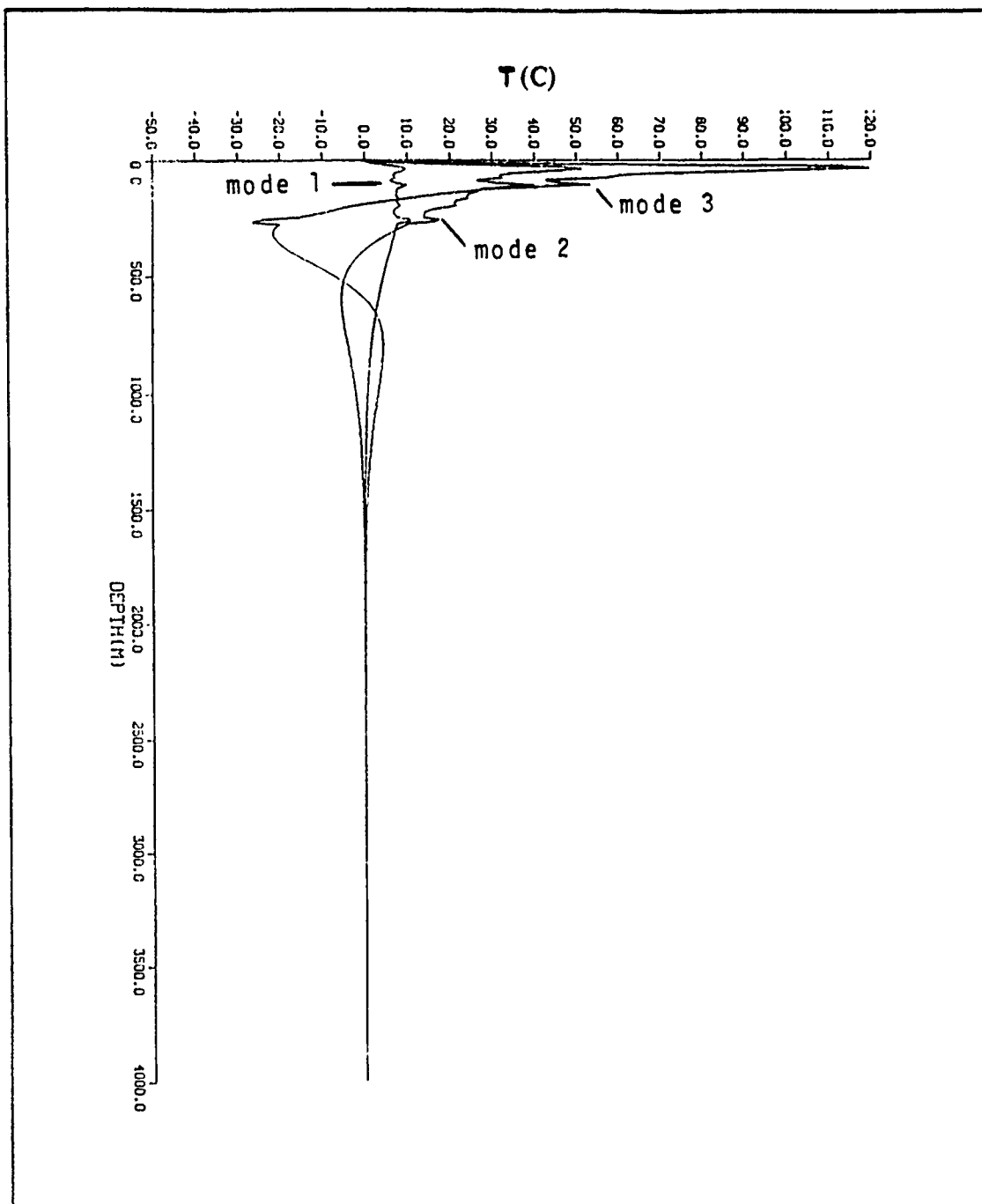
Figure 47.   Plot of Dynamical Modes Versus Depth, Cruise CTZR2

V. DISCUSSION OF RESULTS

Arnone *et al.*, (1990) describes the divergence/upwelling and convergence/downwelling phenomena as observed in the Gulf Stream system via acoustic imaging of biological and physical processes within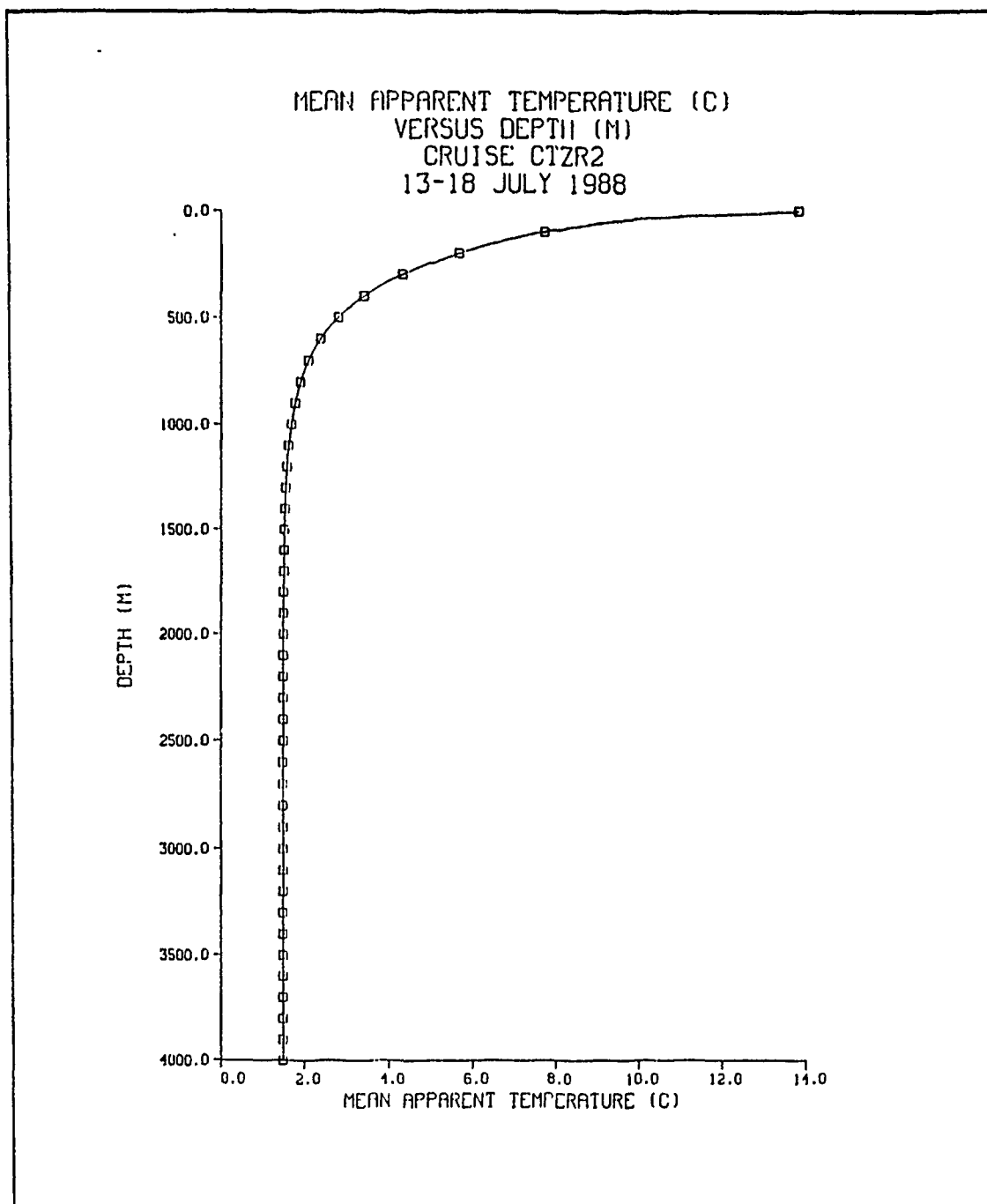 Gulf Stream meanders. Evidently the same divergence/upwelling and convergence/downwelling phenomena is present in the CTZ. To gain some physical insight into the relationships described in Arnone *et al.*, (1990), begin with the two horizontal momentum equations without friction:

$$\frac{du}{dt} - fv = -\alpha \frac{\partial P}{\partial x}, \qquad \{13\}$$

and

$$\frac{dv}{dt} + fu = -\alpha \frac{\partial P}{\partial y}. \qquad \{14\}$$

After cross-differentiating , subtracting the top equation from the bottom equation, and doing appropriate scaling analysis, the following simplified form of the absolute vorticity equation results:

$$\frac{d}{dt}(\zeta + f) = -f\nabla \cdot \vec{V}_H \qquad \{15\}$$

If divergence ($\nabla \cdot \vec{V}_H > 0$) is present, then the absolute vorticity tendency is negative, which implies a tendency for anticyclonic motion. If convergence ($\nabla \cdot \vec{V}_H < 0$) is present, then the absolute vorticity tendency is positive, which implies a tendency for cyclonic motion. To aid in visualizing the preceding discussion, Figure 48 is presented.

To conserve mass, the upwelling centers are located in areas of divergence situated between the upstream trough and downstream ridge. Similarly, the downwelling centers are located in areas of convergence between the upstream ridge and downstream trough.

Rewriting $\frac{d}{dt}(\zeta + f) = -f\nabla \cdot \vec{V}_H$ as $\frac{d}{dt}(\zeta + f) = f\frac{\partial w}{\partial z}$ from continuity, then negative absolute vorticity tendency implies $\frac{\partial w}{\partial z} < 0$, or upwelling. Similarly, positive absolute vorticity tendency implies $\frac{\partial w}{\partial z} > 0$, or downwelling.

The magnitude of upwelling/downwelling in the CTZ can be approximated by doing
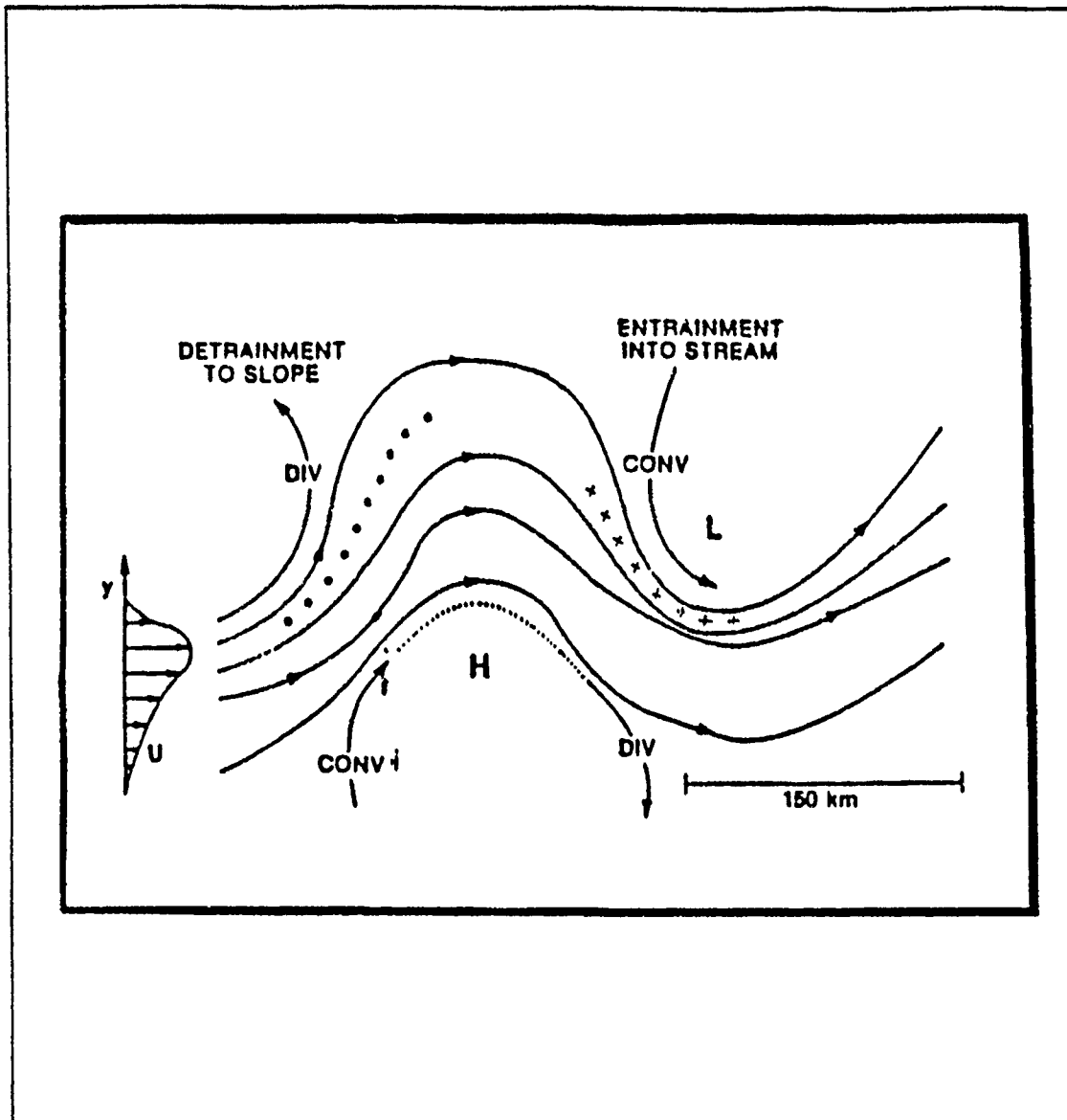
Figure 48.   Convergence and Divergence Patterns in a Typical Meander: Stream-
lines   of   a   typical   meander   showing   the   positions   of   the
divergence/upwelling centers and the convergence/downwelling centers.
Vertical upwelling centers are shown as the fluid enters the crest in the
divergent region (dots), and downwelling centers or convergence are
shown as the fluid enters the trough (crosses) (from Arnone *et al.*,
1990).

a scale analysis of the $f\frac{\partial w}{\partial z}$ term in the equation above.

Now let

$$f\frac{\partial w}{\partial z} \simeq f\frac{w_{-H}}{H} \qquad \{16\}$$

where

f is the coriolis parameter,

w_{-H} is the vertical velocity estimate at depth H, and

H is the depth of interest (100 m).

Continuing,

$$\frac{U^2}{L^2} \simeq f\frac{w_{-H}}{H} \Rightarrow w \simeq R_o\frac{HU}{L} \qquad \{17\}$$

where $R_o = \frac{U}{fL}$, the Rossby number.

Based on an initial estimate of

$$U \sim 10\ cm\ sec^{-1}$$

the fluctuating velocity averaged over the upper 100 m,

$$L \sim 10\ km$$

one-fourth wavelength of upwelling/downwelling pattern,

$$f \sim 10^{-4}\ sec^{-1}$$

and

$$H \sim 100\ m$$

then

$$R_o \sim 0.1$$

and

$$\frac{H}{L} \sim 0.01$$

60

to estimate the vertical velocity as

$$w \sim (.1)(.01)(10) \sim .01 cm\, sec^{-1}$$

or about 10 m day^{-1}, which agrees with the upper estimate of Washburn $et\ al.$, (1990). The vertical velocity magnitudes from CTZR1 model output are 30 to 60 times larger than the above estimate from scale analysis. The cause of such large differences between estimates of vertical velocity based on observations and model output is the topic of a future study.

The "spottiness" of the points identified as downwelling areas is now addressed. Washburn $et\ al.$, (1990) estimated the rate of subduction occurring along the 25.8 and 26.2 density surfaces as six to ten m day^{-1} and two to four m day^{-1}, respectively. The points shown by Washburn $et\ al.$, (1990) in Figure 41 can be considered as points along the subduction path, not isolated vertical columns of upwelling or downwelling. At 20 nm grid spacing between the alongshore legs, exact points of downwelling and upwelling can not be pin-pointed by the model; thus, the areas of downwelling and up-welling must be considered as part of larger mesoscale features, not specific points of vertical sinking or rising motion. A future study should attempt to verify model results with observed downwelling and upwelling areas at specific locations and times; that is, model runs should be integrated forward in time until the time of a recorded observation (or set of observations) is reached, and then the model downwelling and upwelling areas should be compared to downwelling and upwelling areas identified from observations. In this way, a more rigorous verification can be accomplished. Acknowledging the facts that the data points shown in Figure 41 and Figure 42 (top figure) cover all six days of CTZR1, and that the points are not identified by specific dates and times, it is still remarkable that 26 of 33 observed downwelling points occur on model downwelling areas. Similar statements apply to the CTZR2 and CTZ2 data points.

This initial qualitative verification certainly enlivens the possibility that a more rig-orous verification in a future study will show an even higher percentage of observed downwelling or upwelling areas agreeing with respective model results.

61

VI. CONCLUSIONS

The quality of data acquired during cruise CTZR1 is sufficiently high to enable diagnosis of the vertical velocity field using a numerical model. Deeper CTD casts (ideally to the bottom of the ocean for each station) would enable determination of the first three dynamical modes for use in extrapolation of temperature data to the ocean bottom. Only modes two and three could be computed with casts to 500 m. Attempting to extrapolate the apparent temperature to deep depths using data only available to 250 m evidently results in unusually high vertical velocity rates due to an inaccurate representation of the deep mean temperature profile, which is used to calculate the dynamical modes.

The sign of the vertical velocity agrees very well with independent estimates from Washburn *et al.*, (1990). Although the model vertical velocity field and Washburn's data may not be exactly in phase because the data is only quasi-synoptic in time, the high percentage of points (75%) identified to be in downwelling areas which occurred in model output downwelling areas gives confidence to this verification. The results are certainly encouraging and merit further careful study.

The magnitude of vertical velocity in the numerical model is 30 to 60 times larger than the estimated vertical velocity based on observations from Washburn *et al.*, (1990). This basic study used a flat bottom with no forcing other than the initial density field (as reflected in the apparent temperature field used to initialize the model). A future study with variable topography and wind forcing incorporated into the model is necessary to determine their effect on the magnitude of model output vertical velocity.

The ADCP velocity sections showed more detail at deeper depths than the model velocity sections, which showed broader flow at depth and a level of no motion near 300 m. The inclusion of the barotropic mode into the model should improve the resolution of deep flows in model velocity sections. The ADCP and model output velocity sections most closely resembled each other in the vicinity of the core of the jet. Differences between the ADCP and model output velocity cross-sections were more pronounced in areas further from the jet core.

The maximum surface velocities from model and ADCP cross-sections agreed to within 10 cm sec^{-1} except for leg G, in which the ADCP velocity was greater than the model velocity by about 30 cm sec^{-1}. Higher velocities were expected near leg G because

of the higher pressure gradient in the area, and the ADCP acquired data certainly revealed this expectation to be true.

Future work would include the statistical verification of model velocities and ADCP velocities, the incorporation of the barotropic mode into the model, the use of variable topography in the model, and the inclusion of wind stress and surface heat fluxes in the model. The correlation function used in the objective analysis of the CTZ data sets caused instabilities in the objectively analyzed fields which required a convective adjustment before initiation of the model run. The determination of a more optimal correlation function for the data acquired in the CTZ mapping cruises is necessary to fully utilize the data sets.

The results of this study are encouraging first steps in the eventual determination of mass-conserving velocities from numerical models initialized with quasi-synoptic data.

REFERENCES

Arnone, R. A., R. W. Nero, J. M. Jech, and I. De Palma, 1990: Acoustic imaging and biological and physical processes within Gulf Stream meanders. *EOS, 71,* 982.

Bretherton, F. P., R. E. Davis and C. B. Fandry, 1976: A technique for objective analysis and design of oceanic experiments applied to MODE-73. *Deep Sea Res., 23,* 559-582.

Brink, K. H., 1983: The near-surface dynamics of coastal upwelling. *Prog. Oceanog., 12,* 223-257.

Carter, E. F. and A. R. Robinson, 1987: Analysis models for the estimation of oceanic fields. *J. Atmos. Ocean. Tech., 4,* 49-74.

Chelton, D. B., 1984: Seasonal variability of alongshore geostrophic velocity off central California. *J. Geophys. Res., 89,* 3473-3486.

Coastal Transition Zone Group, 1988: The coastal transition zone program. *EOS, 69,* 698, 699, 704, 707.

Errico, R. M., 1989: Theory and application of nonlinear normal mode initialization. *NCAR Technical Note NCAR/TN-344+1A,* National Center for Atmospheric Research, Boulder, Colorado, 137 pp.

Flament, P., L. Armi and L. Washburn, 1985: The evolving structure of an upwelling front. *J. Geo. Res., 90,* 11765-11778.

Foster, K. W., 1989: *Local Area Forecaster's Handbook.* Naval Oceanography Command Facility, San Diego, 116 pp.

Gandin, L. S., 1965: *Objective Analysis of Meteorological Fields.* U. S. Dept. of Commerce, Clearing House for Federal Scientific and Technical Information. 242 pp.

Gill, A. E., 1982: *Atmosphere-Ocean Dynamics.* Academic Press, Inc., 662 pp.

Haney, R. L., 1974: A numerical study of the response of an idealized ocean to large-scale surface heat and momentum flux. *J. Phys. Oceanogr., 4,* 145-167.

--------, 1985: Midlatitude sea surface temperature anomalies: a numerical hindcast. *J. Phys. Oceanogr., 15,* 787-799.

Hickey, B. M., 1979: The California current system: hypothesis and facts. *Prog. in Oceanogr., 8,* 191-279.

Huyer, A. and R. L. Smith, 1974: A subsurface ribbon of cool water over the continental shelf off Oregon. *J. Phys. Oceanogr., 4,* 381-391.

--------, 1983: Coastal upwelling in the California current system. *Prog. Oceanog.,* *12,* 259-284.

--------, P. M. Kosro, J.Fleischbein, S. R. Ramp, T. P. Stanton, L. Washburn, F. Chavez, and T. Cowles, 1990: Currents and water masses of the coastal transition zone off northern California, June to August 1988. *J. Geo. Res.,* submitted.

Ikeda, M. and W. J. Emery, 1984: Satellite observations and modeling of meanders in the California current system off Oregon and northern California. *J. Phys. Oceanogr.,* *14,* 1434-1450.

Jessen, P. F., S. R. Ramp and C. A. Clark, 1989: *Hydrographic Data from the Pilot Study of the Coastal Transition Zone (CTZ) Program 15 - 28 June 1987, NPS-69-89-004,* Naval Postgraduate School, Monterey, CA, 245 pp.

-------- and S. R. Ramp, 1988: Velocity structure associated with a cold filament off Point Arena, California during July 1988. *EOS, 69,* 1259.

Kosro, P. M. and A. Huyer, 1986: CTD and velocity surveys of seaward jets off northern California, July 1981 and 1982. *J. Geo. Res., 91,* 7680-7690.

Lynn, R. J. and J. J. Simpson, 1987: The California current system: the seasonal variability of its physical characteristics. *J. Geo. Res., 92,* 12947-12966.

Mooers, C. N. K., C. A. Collins, and R. L. Smith, 1976: The dynamic structure of the frontal zone in the coastal upwelling region off Oregon. *J. Phys. Oceanogr., 6,* 3-21.

Moum, J. N., D. R. Caldwell and P. J. Stabeno, 1988: Mixing and intrusions in a rotating cold-core feature off Cape Blanco, Oregon. *J. Phy. Ocean., 18,* 823-833.

Paduan, J. D. and P. P. Niiler, 1990: A Lagrangian description of motion in northern California coastal transition filaments. *J. Geo. Res.,* submitted.

Pond, S. and G. L. Pickard, 1983: *Introductory Dynamic Oceanography.* Pergamon Press, Ltd., 241 pp.

Ramp, S. R. and P. F. Jessen, 1988: Preliminary results from the coastal transition zone (CTZ) mapping cruises during July 1988. *EOS, 69,* 1259.

Rienecker, M. M., C. N. K. Mooers and A. R. Robinson, 1987: Dynamical interpolation and forecast of the evolution of mesoscale features off northern California. *J. Phys. Oceanogr., 17,* 1189-1213.

-------- and C. N. K. Mooers, 1989: Mesoscale eddies, jets, and fronts off Point Arena, California, July 1986. *J. Geo. Res., 94,* 12555-12569.

Ross, B. B. and I. Orlanski, 1982: The evolution of an observed cold front. Part I: numerical simulation. *J. Atmos. Sci., 39,* 296-327.

Sarmiento, J. L. and K. Bryan, 1982: An ocean transport model for the north Atlantic. *J. Geo. Res., 87,* 394-408.

Simpson, J. J., C. J. Koblinsky, L. R. Haury, and T. D. Dickey, 1984: An offshore eddy in the California current system: preface. *Prog. Oceanog., 13,* 1-4.

--------, C. J. Koblinsky, L. R. Haury, and T. D. Dickey, 1984: An offshore eddy . the California current system. Part I: interior dynamics. *Prog. Oceanog., 13,* 5-49.

Smith, J. A., 1984: *Empirical and dynamic modes in the CCS, NPS68-84-003,* U. S. Naval Postgraduate School, 42 pp.

Stanton, T. P. and J. Stockel, 1988: Relaxation of the CTZ 88 domain. *EOS, 69,* 1260.

Tchernia, P., 1980: *Descriptive Regional Oceanography.* Pergamon Press Inc., 253 pp.

Tibby, R. B., 1941: The water masses off the west coast of North America. *J. Mar. Res., 4,* 112-121.

von Schwind, J. J., 1980: *Geophysical Fluid Dynamics for Oceanographers.* Prentice-Hall, Inc., 307 pp.

Washburn, L., D. C. Kadko, B. H. Jones, T. Hayward, P. Michael Kosro, T. P. Stanton, A. Huyer, S. R. Ramp, and T. Cowles, 1990: Water mass subduction and the transport of phytoplankton in a coastal upwelling system. (manuscript)

INITIAL DISTRIBUTION LIST

No. Copies

1. Defense Technical Information Center 2
   Cameron Station
   Alexandria, VA 22304-6145

2. Library, Code 52 2
   Naval Postgraduate School
   Monterey, CA 93943-5002

3. Chairman (Code OC/Co) 1
   Department of Oceanography
   Naval Postgraduate School
   Monterey, CA 93943-5000

4. Chairman (Code MR/Hy) 1
   Department of Meteorology
   Naval Postgraduate School
   Monterey, CA 93943-5000

5. Professor Timothy P. Stanton (Code OC/St) 1
   Department of Oceanography
   Naval Postgraduate School
   Monterey, CA 93943-5000

6. Professor Steven R. Ramp (Code OC/Ra) 1
   Department of Oceanography
   Naval Postgraduate School
   Monterey, CA 93943-5000

7. Professor I. M. Navon 1
   Department of Mathematics
   Florida State University
   Tallahassee, FL 32306-4052

8. Dr. Francisco Chavez 1
   MBARI
   160 Central Avenue
   Pacific Grove, CA 93950

9. LT. James R. Mallette 1
   NPS Code 35
   U. S. Naval Postgraduate School
   Monterey, CA 93950

10. Commander   1
    Naval Oceanography Command
    Stennis Space Center
    MS 39529-5000

11. LCDR Roland E. de Jesus   1
    NOCC/JTWC COMNAVMARIANAS
    Box 12
    FPO San Francisco, CA 96630

12. Mr. and Mrs. Wilfrido G. de Jesus   1
    733 Coleman Court
    San Diego, CA 92154

13. Mr. and Mrs. Edgardo N. Garcia   1
    1940 Oro Vista Road
    San Diego, CA 92154